STUDIES ON DEFORMATION AND SOLVENT PERMEATION OF POLYMER GELS INDUCED BY EXTERNAL FORCES

SHOJI NOSAKA

2007

CONTENTS

Chapter 1

General Introduction

Polymer gels are one of the soft materials that are familiar in our life. For example, jellies and agars are typical polymer gels.[1-3] Polymer gels are the polymer networks swollen by a considerable amount of solvent and that have unique natures. Gels possess a high water retentivity as well as an water absorption capability, i.e., the absorbed water is not easily expelled from the gels compared with sponges. The high solvent-absorption ability of dried gels is applied to sanitary napkins and diapers.[4-6] The water retentivity of gels is applied in the field of agriculture.[7,8] Some polymer gels behave as stimuli responsive materials. These gels largely vary the volume in response to external stimulus, such as the changes in temperature, pH and solvent composition. These gels are expected as intelligent materials owing to the unique stimulus-response behavior, and they are used in various areas, for example, drug delivery system (DDS),[9-11] gel actuators[12] and so on. See in our body, biological gels[13-15] can be found throughout our body.

Polymer gels consist of three-dimensional polymer networks and solvent.[16, 17] Polymer gels can be classified into some types according to solvent types. The gels swollen by organic solvent (for instance methanol, hexane and acetone) or water are called organogels or hydrogels, respectively. The gels with no solvent, namely dried polymer networks, called xerogels. The gels can also be categorized on the basis of the types of cross-links: One is physical gel whose cross-links are made by noncovalent bands, typically ionic bonds, hydrogen

bonds and microcrystallites. The other is chemical gel whose cross-links are covalent bonds. The structure of the physical cross-links formed by intermolecular interactions would be affected by various environmental factors such as temperature, quality of solvent and applied stresses. In contrast, the covalent bonds are stable unless the degradations occur or excessive stress is applied. Recently, the gel called slide-ring gel with new type of cross-links has been reported.[18-21] The cross-links of the slide-ring gel are mobile because they are designed as a figure of eight and the main linear chains pass through the rings of the cross-links. The both ends of the main chains have a bulky structure to prevent the chains from escaping from the rings. The numerous combinations of the solvent and network as well as the several types of cross-links lead to a wide variety of gels. This extends the possibility and application of the gels.

Swelling of polymer gels in solvent is affected by a change of the external factors such as temperature, pH of solvent. The swelling equilibrium is achieved by the balance of the chemical potentials of the solvents inside and outside the gel. The thermodynamics of the swelling of polymer networks in solvents has been described by extending that of the mixing of uncrosslinked polymers and solvents.[16] The polymer networks with infinite molecular weight exhibit the rubber elasticity, and it significantly contributes to the free energy of the systems. When the neutral networks with no ionic groups are soaked in solvent, the change of Gibbs free energy (ΔG) is written as the sum of a contribution of the mixing of the polymer network and the solvent (ΔG_m) and a contribution of the elasticity of the network (ΔG_e).[16, 22-24]

$$\Delta G = \Delta G_m + \Delta G_e \qquad (1.1)$$

For polymer networks with ionic groups, the effect of the ionic interaction must also be taken into account. The energy of mixing ΔG_m is calculated on the basis of the lattice model, and the energy of elasticity ΔG_e is described by the theory of the rubber elasticity. These are written as

$$\Delta G_m = n_S k_B T\left[\ln(1-\phi)+\chi\phi\right] \tag{1.2}$$

$$\Delta G_e = (3/2)N_C k_B T\left(\alpha^2 - 1 - \ln\alpha\right) \tag{1.3}$$

where n_S, k_B, T and N_C represent the number of solvent molecules, Boltzmann constant, temperature and the number of the effective elastic chain, respectively. The quantities ϕ and α depict the volume fraction of polymer network and the principal ratio of the network, respectively, and they are related as $\alpha = (\phi_0 / \phi)^{1/3} = (V / V_0)^{1/3}$, where V represents the volume of the polymer gel and the subscript "0" means the initial state before swelling. The quantity χ stands for the mixing interaction parameter between solvent and polymer network, and it is a measure of the quality of the solvent for the network. By rewriting Equations (1.1-1.3), we can regard the equilibrium as the balance of the two types of osmotic pressure, i.e. a pressure caused by mixing of the solvent and polymer networks ($\Delta\Pi_m$) and that by the elastic force of the networks ($\Delta\Pi_e$):[16, 22-24]

$$\Delta\Pi = -\left(\frac{\partial(\Delta G)}{\partial V}\right)_T = \Delta\Pi_m + \Delta\Pi_e = 0 \tag{1.4}$$

$$\Delta\Pi_m = -\frac{k_B T}{v_S}\left[\phi + \ln(1-\phi) + \chi\phi^2\right] \tag{1.5}$$

$$\Delta\Pi_e = N_C k_B T\left[\frac{\phi}{2\phi_0} - \left(\frac{\phi}{\phi_0}\right)^{1/3}\right] \tag{1.6}$$

where v_S stands for the volume of the solvent molecule. Swelling behavior of the polymer gel affected by external stimuli can be explained as follows: A external stimulus imposed on the equilibrium swollen gel results in an additional finite osmotic pressure ($\Delta\Pi \neq 0$). It causes a shift of the swelling equilibrium, and ϕ increase or decrease until $\Delta\Pi = 0$ is achieved.

It is well known that some polymer gels undergo the volume phase transition.[22-29] The volume phase transition is the phenomena that polymer gels show the discontinuous volume changes in response to the infinitesimal variation of the external factors such as pH, temperature or composition of the solvent. This phenomena was firstly found by Tanaka et al. in the experiments for polyacrylamide (PAAm) gels in acetone / water mixed solvents.[22] The gels underwent a collapse with increasing the acetone concentration or decreasing temperature. They discussed the volume phase transition on the basis of the Flory's formula, namely by using Equations (1.1-1.6). The volume phase transitions of various polymer gels have been demonstrated, and it has been revealed that the volume phase transition often occurs for the ionic polymer networks.[25, 26]

Poly(*N*-isopropylacrylamide) (PNIPA) hydrogels and its derivatives with hydrophobic groups in the networks have been investigated as non-ionic polymer hydrogels that undergoes discontinuous volume change in response to infinitesimal change of temperature.[23, 24] The transition temperature (T_{tr}) of the gels is around 33 ^{o}C. Below T_{tr} the gel is swollen by a lot amount of water and above T_{tr} the gels collapse. This is opposite to the behavior of PAAm gels in mixed solvents: The PAAm gel is swollen at high temperatures and collapsed at low temperatures. This is attributed to the state of water that forms an ordered

structure near the hydrophobic chains.[27] The ordered structure of water covers the hydrophobic chains to stabilize these chains that can not be dissolved in water. Increasing temperature causes destruction of the protecting structure and the hydrophobic chains are aggregated each other. In this process, the increase in entropy by randomized water molecules and the decrease in entropy by the aggregation of the chains occur simultaneously. The total entropy increases because the increase of the entropy exceeds the decrease. This is the mechanism of the volume phase transition of PNIPA hydrogels in pure water and is called hydrophobic interaction. The volume phase transitions of both ionic and non-ionic polymer gels attract much attentions, and the ability of the large volume change in response to external stimuli is applied to various fields.

Swelling and deswelling kinetics of polymer gels have also been investigated by many researchers.[30-39] Various kinetic models have been proposed. In case of the swelling dynamics measurements for dried glassy samples, swelling as well as plasticization of the samples simultaneously occurs. Thus some glassy gels show complicated swelling dynamics.[37-39] In the swelling dynamics of the rubbers and sufficiently swollen gels, the swelling mechanism is entirely attributed to collective diffusion of polymer networks. Tanaka et al.[30] proposed the diffusion equation of the spherical gels on the basis of the equation of motion of polymer network swollen in solvent. The solution was a multi-exponential function with the longest characteristic time τ given by

$$\tau = \frac{r_\infty^2}{\pi^2 D} \tag{1.7}$$

with

$$D = \frac{K + 4/3\,G}{f} \tag{1.8}$$

where r_∞ and D stands for equilibrium radius of spherical gel and the diffusion constant, and K, G and f represent osmotic bulk modulus, shear modulus and frictional coefficient between solvent and polymer network. Equation (1.7) indicates that the characteristic time of the swelling greatly depends on the dimensions of the gel, i.e., proportional to the square of r_∞. The swelling experiments using the spherical gels confirmed the validity of the theory. The kinetic theory was extended for long cylindrical gels and large disk gels with shape anisotropy.[33] The theoretical predictions agreed well with the experimental results. The swelling kinetics of polymer gels is very important in the application of polymer gels.

Frictional coefficient f between the polymer networks and the solvent is one of the important parameters that determine the swelling kinetics as shown in Equation (1.8). The physical meaning of f is evident, but the measurements of f have been reported in only a few literatures due to the experimental difficulty.[40-42] Tokita et al.[40] successfully measured f of transparent PAAm hydrogels by solvent permeation through the gels, and they reported that f depends on the polymer concentration C as $f \propto C^{1.5}$. They also found that f for opaque polyacrilamide gels with a inhomogeneous structure due to the high cross-link density is far smaller than that of transparent gels.[41] In another solvent permeation experiments,[42] it has been reported that the volume change of polymer gels is induced by solvent flow. Polymer gels are expected as materials with separability of mixtures. In the separation technique using permeation through polymer gels, f is one of the most important parameter because the

permeation of the solvent and the dissolved substances would be controlled by f. Thus the studies of the solvent permeation behavior are useful for a separation technique. However, the permeation behavior of the mixed solvents through gels has not been reported even though the system is simple. The experimental characterizations of the solvent permeation through gels are needed as a basis for the applications to the separation technique.

Swollen polymer gels possess a rubber elasticity. The gels can be largely deformed by small forces, and the deformation is reversible when repeating the cycle of loading and unloading. This nature of polymer gels is applied to mechanical devices such as actuators and artificial muscles. It should be noted that the imposed deformation considerably affects the degree of the swelling. The studies of swelling behavior of polymer gels under deformation are very important for these applications. The swelling behavior of deformed gels has been experimentally and theoretically investigated.[43-49] When a stress or strain is applied to a gel in the equilibrium state, the gel changes the swelling ratio by the shift of the equilibrium state that is caused by the change of the elastic energy of the network by elongation or compression. This is called "stress-diffusion coupling phenomena" and gathers attention in the science of polymer gels.[50-54] The Poisson's ratio μ is a convenient parameter to characterize the degree of the swelling induced by the imposed deformation. When a stress or a strain is applied to a gel in the x-direction, μ is defined as

$$\mu = -\frac{\varepsilon_i}{\varepsilon_x} \qquad (i = y, z) \tag{1.9}$$

where ε stands for the strain and the subscript denotes means the principal direction: y and z-directions are perpendicular to the applied force. When the

volume of the material is unchanged before and after deformation, (i.e., the material is mechanically incompressible) μ is 1/2. In general, when a stress or a strain is applied to swollen gels, firstly the gels undergo an instantaneous deformation like the elastic deformation of rubbers. The corresponding Poisson's ratio for this initial deformation (μ_0) is near 0.5, namely little volume change occurs. Then the volume of the gels is changed with increasing time by the slow diffusion process, and it reaches the equilibrium in the long time limit. The Poisson's ratio in the equilibrium state is called osmotic Poisson's ratio (μ_∞). A theory[44] for the deformed gel in good solvent predicted that μ_∞ = 1/6 that agreed with the experimental results. In the earlier studies of swelling behavior of the deformed gel, the gel in the swollen state were employed as a sample. In contrast, the swelling behavior of the deformed gel in the collapsed state (i.e., the gel in poor solvent) remains still unclear. The mechanical properties of the polymer gels depends on the change of the swelling degree. For example, elastic moduli of the gels in swollen state are considerably different from that of collapsed gels.

The main aim of this study is to investigate the swelling and shrinking behavior of polymer gels under various external forces. A new method to measure some physical properties of polymer gels related with the swelling property is proposed and the physical constants that have not been well characterized are quantitated. Solvent flow property through polymer gels is also examined for the binary solvent system.

In Chapter 2, a new type of rheometer called "a magnetic force driven rheometer" is developed to observe the swelling behavior of polymer gels under dynamic (sinusoidal) stresses. The swelling behavior of cylindrical PNIPA

hydrogels under dynamic stresses is investigate at the temperature below the transition temperature. The dependence of the volume change on the frequency of applied stresses is examined. In addition, the swelling under static (constant) stresses is also investigated. The correlation between the dynamic and static results are discussed.

In Chapter 3, the swelling behavior of PNIPA gels in the collapsed state is investigated. The dynamic and static stresses are applied to the gels above the transition temperature and the swelling behavior is observed by the same methodology in Chapter 2. The different behavior between collapsed and swollen gels are discussed from the point of view of the difference in the cross-linking structure. The correlation of the deformation behaviors under dynamic and static stresses are elucidated.

In Chapter 4, the shrinking behavior of the polymer gels under ultracentrifugal forces are investigated. Ultracentrifuges have been used in studies of the dilute polymer solution, in particular in order to evaluate the molecular weight of the polymer. The theoretical background for the sedimentation equilibrium and sedimentation velocity have been well established for the polymer solutions. Instead of polymer solution, PAAm gels are settled in ultracentrifugal fields and the shrinkage of the gels by centrifugal forces are observed. A theory which explains the shrinkage is proposed and is compared with the experimental results.

In Chapter 5, the shrinking behavior of poly(vinyl alcohol) gels by ultracentrifugal forces are investigated. Polyacrylamide gels used in the previous chapter are classified into chemical gels. In this chapter, poly(vinyl alcohol) gels that are physical gels with physical cross-linking by intermolecular interactions

are employed as the samples. The experimental results is analyzed with the same theory and the availableness and universality of this analysis method is examined. In addition, the rotational speed dependence of the shrinking velocity of the gels are investigated.

In Chapter 6, the mixed solvent flow properties through gel membranes are investigated. A simple model for binary solvent systems is proposed by extending the existing theory for the flow-induced swelling. A combination of PNIPA gels and mixed solvent of water / dimethylformamide is employed and the solvent flow properties are studied. In addition, a possibility of a separation of mixed solvent by using polymer gel membrane is discussed

References

1. F. Warin, V. Gekas, A. Voirin, and P. Dejmek, *J. Food Sci.*, **62**, 454 (1997)
2. C. Calvo, and A. Salvador, *Food Hydrocoll.*, **14**, 439 (2000)
3. A. Igarashi, E. Arai, R. Watanabe, Y. Miyaoka, T. Tazawa, H. Hirano, S. Nomura, and Y. Yamada, *J. Texture Stud.*, **33**, 285 (2002)
4. S. S. Cutié, and S. J. Martin, *J. Appl. Polym. Sci.*, **55**, 605 (1995)
5. F. L. Buchholz, S. R. Pesce, and C. L. Powell, *J. Appl. Polym. Sci.*, **98**, 2493 (2005)
6. F. Hua, and M. Qian, *J. Mater. Sci.*, **36**, 731 (2001)
7. S. Ouchi, A. Nishikawa, and F. Fujita, *Jpn. Soc. Soil Sci. Plant Nut.*, **60**, 15 (1989)
8. KS Kazanskii, and SA Dubrovskii, *Adv. Polym. Sci.*, **104**, 97 (1992)
9. "*Polymer Gels : Fundamental and Biomedical Applications*", D. DeRossi, K. Kajiwara, Y. Osada, and A. Yamauchi, Ed., Plenum Press, New York, 1991
10. N. Kubota, T. Matsubara, and Y. Eguchi, *J. Appl. Polym. Sci.*, **70**, 1027 (1998)
11. T. Okano, Y.H. Bae, H. Jacobs, and S.W. Kim, *J. Control. Rel.*, **11**, 255 (1990)
12. T. Hirai, H. Nemoto, M. Hirai, and S. Hayashi, *J. Appl. Polym. Sci.*, **53**, 79 (1994)
13. K. Bohon, and S. Krause, *J. Polym. Sci., Part B: Polym. Phys.*, **36**, 1091 (1998)
14. A. Kakugo, S. Sugimoto, J. P. Gong, and Y. Osada, *Adv. Mater.*, **14** 1124

(2002)

15. M. Oka, K. Ushio, P. Kumar, K. Ikeuchi, S. H. Hyon, T. Nakamura, and H. Fujita, *Proc. Instn. Mech. Engrs., Part H*, **214**, 59 (2000)
16. P. J. Flory, "*Principles of Polymer Chemistry*", Cornell University Press, Ithaca, NY, 1953
17. P. G. de Gennes, "*Scaling Concepts in Polymer Physics*", Cornell University Press, Ithaca and London, 1979
18. Y. Okumura, and K. Ito, *Adv. Mater.*, **13**, 485 (2001)
19. T. Karino, Y. Okumura, K. Ito, and M. Shibayama, *Macromolecules*, **37**, 6177 (2004)
20. T. Karino, Y. Okumura, C. Zhao, T. Kataoka, K. Ito, and M. Shibayama, *Macromolecules*, **38**, 6161 (2005)
21. T. Karino, M. Shibayama, and K. Ito, *Physica B*, **385/386**, 692 (2006)
22. T. Tanaka, *Phys. Rev. Lett.*, **40**, 820 (1978)
23. S. Hirotsu, *J. Phys. Soc. Jpn.*, **56**, 233 (1987)
24. S. Hirotsu, *J. Chem. Phys.*, **88**, 427 (1988)
25. T. Tanaka, D. Fillmore, S. Sun, I. Nishio, G. Swislow, and A. Shah, *Phys. Rev. Let.*, **45**, 1636 (1980)
26. S. Hirotsu, Y. Hirokawa, and T. Tanaka, *J. Chem. Phys.*, **87**, 1392 (1987)
27. Y. Hirokawa, and T. Tanaka, *J. Chem. Phys.*, **81** 6379 (1984)
28. M. Shibayama, and T. Tanaka, *Adv. Poly. Sci.*, **109**, 1 (1993)
29. A. Onuki, *Adv. Poly. Sci.*, **109**, 63 (1993)
30. T. Tanaka, and D. J. Fillmore, *J. Chem. Phys.*, **70**, 1214 (1979)
31. A. Peters, and S. J. Candau, *Macromolecules*, **19**, 1952 (1986)
32. A. Peters, and S. J. Candau, *Macromolecules*, **21**, 2278 (1988)

33. Y. Li, and T. Tanaka, *J. Chem. Phys.*, **92**, 1365 (1990)

34. C. Wang, Y. Li, and Z. Hu, *Macromolecules*, **30**, 4727 (1997)

35. E. Sato Matsuo, and T. Tanaka, *J. Chem. Phys.*, **89**, 1695 (1988)

36. C. Hui, and V. Muralidharan, *J. Chem. Phys.*, **123**, 154905 (2005)

37. J. S. Vrentas, C. M. Jarzebski, and J. L. Duda, *AICHE J.*, **21**, 894 (1975)

38. B. A. Firestone, and R. A. Siegel, *J. Appl. Polym. Sci.*, **43**, 901 (1991)

39. R. A. Siegel, I. Jahannes, C. A. Hunt, and B. A. Firestone, *Pharm. Res.*, **9**, 76 (1992)

40. M. Tokita, and T. Tanaka, *J. Chem. Phys.*, **95**, 4613 (1991)

41. Y. Doi, and M. Tokita, *Langmuir*, **21**, 9420 (2005)

42 T. Takigawa, K. Uchida, K. Takahashi, and T. Masuda, *J. Chem. Phys.*, **111**, 2295 (1999)

43. A. Onuki, *J. Phys. Soc. Jpn.*, **57**, 699 (1988)

44. T. Takigawa, K. Urayama, Y. Morino, and T. Masuda, *Polymer Journal*, **25**, 929 (1993)

45. T. Takigawa, T. Yamawaki, K. Takahashi, and T. Masuda, *Polymer Gels and Networks*, **5**, 585 (1997)

46. T. Takigawa, T. Ikeda, Y. Takakura, and T. Masuda, *J. Chem. Phys.*, **117**, 7306 (2002)

47. N. Gundogan, D. Melekaslan, and O. Okay, *Macromolecules*, **35**, 5616 (2002)

48. S. Sasaki, *J. Chem. Phys.*, **120**, 5789 (2004)

49. S. Hirotsu, *Macromolecules*, **37**, 3415 (2004)

50. T. Yamaue, and M. Doi, *Phys. Rev. E*, **69**, 041402 (2004)

51. T. Yamaue, and M. Doi, *Phys. Rev. E*, **70**, 011401 (2004)

52. T. Yamaue, T. Taniguchi, and M. Doi, *Mol. Phys.*, **102**, 167 (2004)

53. T. Yamaue, and M. Doi, *J. Chem. Phys.*, **122**, 084703 (2005)

54. M. Doi, and T. Yamaue, *Phys. Rev. E*, **71**, 041404 (2005)

Chapter 2

Effects of Static and Dynamic Loading on Swelling of Poly(*N*-isopropylacrylamide) Gels in the Swollen State

2.1 Introduction

Polymer gels vary the degree of swelling upon the change of external circumstances as stated in Chapter 1. For example, hydrogels in aqueous media change the volume in response to the variation in temperature, pH, ionic strength, and so on.[1-3] Recently, it has been reported that when the external fields (for example, the mechanical stresses or strains) are applied to the fully swollen gels, the shrinkage or further swelling occurs as a result of a shift of the equilibrium state. The volume change responding to the applied stress originates from the fact that the polymer network and solvent molecules form a thermodynamical semi-open system, and this phenomenon has been called the stress-diffusion coupling.[4] Studies on swelling kinetics of the polymer gels after the application of mechanical stimulus have been made by employing so-called static methods,[5-10] such as continuous monitoring of the gel dimension after imposition of a step stress. They have shown that in the long time region the volume change can be written by a single exponential function; i. e., a single characteristic (or relaxation) time governs the swelling kinetics in that time region. On the other hand, little is known on the swelling kinetics at short times, where a multi-exponential character is considered to become dominant for the volume change.[9, 11] Studies in terms of dynamic viscoelasticity will be very useful to give the full picture of the swelling kinetics of the polymer gels. Conventional

rheometers, however, cannot be used for this purpose; the rheometers require relatively large gel specimens to detect the mechanical response but the relaxation time of such large specimens is far out of the measurable frequency range of the rheometers because the characteristic time for swelling is proportional to square of gel dimensions. A new type of rheomter, applicable to very small gel specimens, is needed to investigate the dynamic swelling properties of polymer gels. In this study we have made a new apparatus to observe the swelling behavior of polymer gels under dynamic loading, and examined the frequency dependence of the dynamic Poisson ratio for the gels.

In this study, poly(*N*-isopropylacrylamide) (PNIPA) gels are employed as samples. As stated in Chapter 1, PNIPA hydrogels undergo the volume phase transition in response to an infinitesimal change in temperature, and the transition temperature (T_t) has been reported to be $T_t \approx 32$ °C: A slight increase in temperature causes a drastic decrease in volume around 32 °C. Below T_t the gels are highly swollen by water and this state is called “swollen state”. Above T_t the gels consist of a very small amount of water, which is called “collapsed gels”, or “gels in the collapsed state”. In this chapter we treat the PNIPA gels in “swollen state”, and the gels in the “collapsed state” will be stated in the next chapter. We have investigated the swelling properties of PNIPA hydrogels in the swollen state under static and dynamic loading and compared the results obtained by the dynamic tests with those by the static tests.

2.2 Definition of Dynamic Variables

Consider a time (t) profile of strain in response to an applied elongational

stress (σ) composed of sum of the static stress σ_S and the dynamic stress σ_D as

$$\sigma = \sigma_S + \sigma_D \tag{2.1}$$

where σ_D is given by $\sigma_D=\sigma_0\exp(i\omega t)$ with the amplitude σ_0 and the angular frequency ω. The strain is defined by the ratio of the change of dimensions to the initial value before deformation. The strains parallel ($\varepsilon_{//}$) and perpendicular ($\varepsilon_{\perp}$) to elongation can be also divided into two components: the static and dynamic strains.

$$\varepsilon_{//} = \varepsilon_{//,S} + \varepsilon_{//,D} \tag{2.2a}$$

$$\varepsilon_{\perp} = \varepsilon_{\perp,S} + \varepsilon_{\perp,D} \tag{2.2b}$$

Within the framework of the infinitesimal deformation theory,[12] the Poisson ratio (μ) is defined in terms of (static) strains as follow equation.

$$\mu = -\frac{\varepsilon_{\perp}}{\varepsilon_{//}} \tag{2.3a}$$

In this study, we define the dynamic Poisson ratio (μ_D) with the dynamic strains as

$$\mu_D = -\frac{\varepsilon_{\perp,D}}{\varepsilon_{//,D}} \tag{2.4b}$$

Phase lags of $\varepsilon_{//,D}$ and $\varepsilon_{\perp,D}$ from the stress wave, $\delta_{//}$ and $\delta_{\perp}$ respectively, are defined with the following equations.

$$\varepsilon_{//,D} = \varepsilon_{//,0}\exp[i(\omega t + \delta_{//})] \tag{2.5a}$$

$$\varepsilon_{\perp,D} = \varepsilon_{\perp,0}\exp[i(\omega t + \delta_{\perp} + \pi)] \tag{2.5b}$$

And the dynamic Poisson ratio defined by Equation (2.4b) can be rewritten as

$$\mu_D = -\frac{\varepsilon_{\perp,0}}{\varepsilon_{//,0}}\exp[i(\delta_{\perp} - \delta_{//} + \pi)] = \frac{\varepsilon_{\perp,0}}{\varepsilon_{//,0}}\exp[i(\delta_{\perp} - \delta_{//})] \tag{2.6}$$

where $\varepsilon_{//,0}$ and $\varepsilon_{\perp,0}$ are the amplitudes of the strains parallel and perpendicular to elongation, respectively. We define $\varepsilon_{\perp,D}$ in consideration of the natural phase lag (π) between the strains parallel and perpendicular resulting in the simple form of the dynamic Poisson ratio without minus sign (Equation (2.6)). It is expected that $\delta_{//}$ and $\delta_{\perp}$ are equal to 0 for the ideal elastic bodies. It is also clear that $-\pi / 2 \leq \delta_{//} \leq 0$ for viscoelastic bodies, but the range of $\delta_{\perp}$ is not explicitly clear, so that we assume $-\pi < \delta_{\perp} \leq \pi$. Equation (2.6) leads to the relation that $|\mu_D| = \varepsilon_{\perp,0} / \varepsilon_{//,0}$. Figure 2-1 shows a schematic representation of $\delta_{//}$ and $\delta_{\perp}$ in the complex plane. To analyze the dynamic data, it is useful to decompose dynamic components into two parts: the in-phase part and the out-of-phase part. For example, $\varepsilon_{//,D}$ and μ_D are decomposed as

$$\varepsilon_{//,D} = \varepsilon'_{//,D} + i\varepsilon''_{//,D} = \varepsilon_{//,0} \cos\delta_{//} + i\varepsilon_{//,0} \sin\delta_{//} \tag{2.7}$$

$$\mu_D = \mu'_D + i\mu''_D = |\mu_D| \cos(\delta_{\perp} - \delta_{//}) + i|\mu_D| \sin(\delta_{\perp} - \delta_{//}) \tag{2.8}$$

where the prime and double prime means the in-phase part and the out-of-phase part, respectively. All the dynamic components can be decomposed into two parts in the same way.

2.3 Experimental

2.3.1 Materials

Poly(*N*-isopropylacrylamide) (PNIPA) gels were prepared by radical copolymerization of *N*-isopropylacrylamide (NIPA) and *N*,*N*'-methylenebisacrylamide (BIS). The reagents, NIPA and BIS, were dissolved in distilled water under nitrogen atmosphere. The total monomer

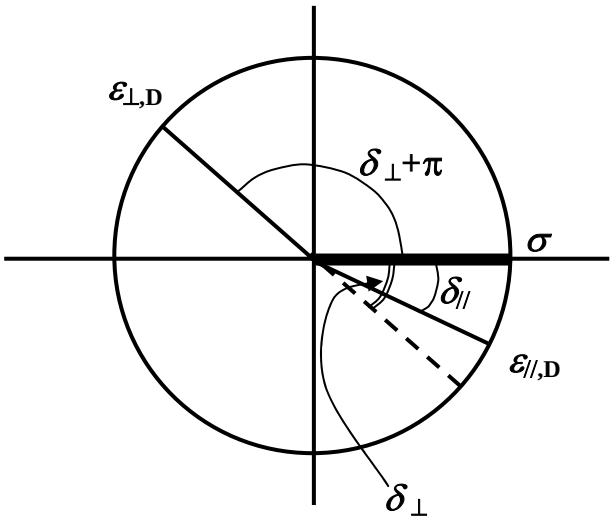

Figure 2-1 A relation between $\delta_{//}$ and $\delta_\perp$ (phase lags for $\varepsilon_{//,D}$ and $\varepsilon_{\perp,D}$ seeing from the stress wave, respectively) in the complex plane with $-\pi / 2 \le \delta_{//} \le 0$ and $-\pi < \delta_\perp \le \pi$.

concentration of NIPA and BIS was fixed to be 13wt%, and the molar ratio [NIPA] / [BIS], which is a measure of the crosslink density, was also fixed to be 53. After ammonium peroxodisulfate (initiator) and *N*,*N*,*N*',*N*'-tetramethylethylenediamine (accelerator) were added into the solution, the pregel solution was transferred into glass capillaries and then the gelation was performed at 5°C. The time for gelation was settled to be 24 hours. The concentrations of AP and TEMED were 0.8 g/l and 2.4 ml/l, respectively. The cylindrical gel samples were removed from the capillaries and were poured into hot distilled water (about 50°C) to eliminate the unreacted reagents. The length and diameter of the swollen gel samples at 25°C were ca. 20 mm and ca. 400μm, respectively.

2.3.2 Measurements

A laboratory-made magnetic force-driven (namely, a stress-controlled type) rheometer was used to investigate the static and dynamic swelling properties of the PNIPA gels. The outline of the apparatus is shown in Figure 2-2. A metal (tungsten carbide) sphere was glued to one end of the gel using a cyanoacrylate-type adhesive. The gel with the metal sphere was put in a glass-made solvent bath comprising inner and outer compartments. The inner compartment, where the gels were immersed, was filled with a surrounding solvent: water (W) or liquid paraffin (LP). However, the solvent in the gels ("inside solvent") was water throughout. The outside solvent LP is a non-solvent for the PNIPA gels.

Temperature-controlled water was circulated in the outer bath to keep temperature constant throughout the experiments. Magnetic force was applied to

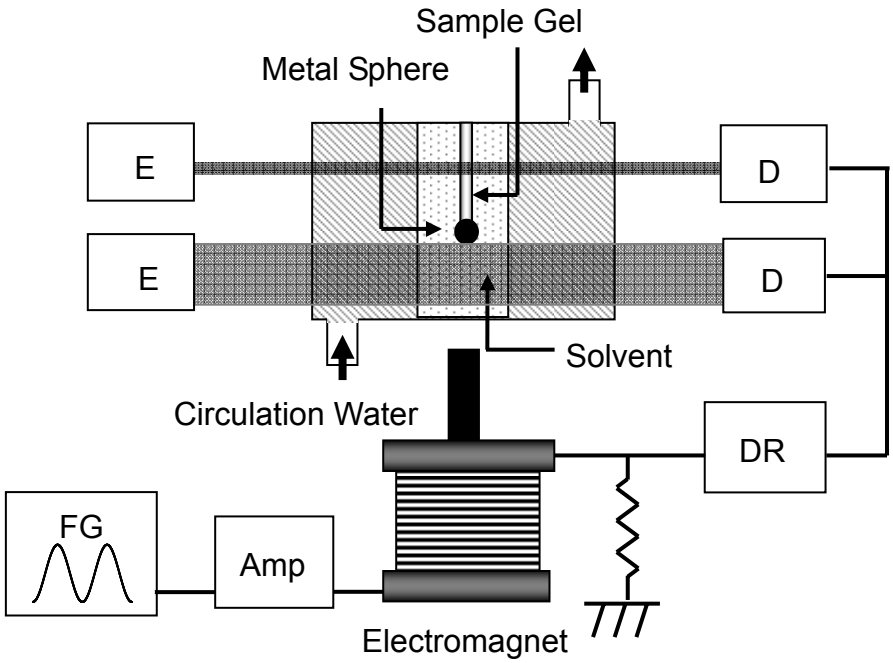

Figure 2-2 Schematic representation of magnetic force-driven rheometer. FG; function generator: Amp; power amplifier: E; emitter part of laser scan micrometer: D; detector of laser scan micrometer: DR; Digital Recorder.

the metal sphere by controlling the current in the coil. The current wave was generated by a NF power amplifier (4010 High Speed Power Amplifier/Bipolar Power Supply) based on the voltage-wave designed by a Yokogawa function generator (FG200). The static stress acting to the gels is originated from DC in the coil, while the dynamic stress comes from AC. The dimension of the gels was measured as a function of time (t) by two sets of emission-detector units (Laser Scan Micrometer; Keyence, LS5500): One monitored the diameter and the other monitored the position of the metal sphere from the bottom of the bath (namely, the length of the gels). The wave-form data from the output of the detectors were recorded with a Yokogawa analyzing recorder (AR1100A) together with the wave-form data of the current in the coil. The swelling of the gels were equilibrated in water at 25°C before the measurements, and thereafter the gels were transferred to the solvent bath of the rheometer.

2.4 Results and Discussion

2.4.1 Static Properties

Figure 2-3 shows the time dependence of dimensions of the gel sample in water after the imposition of the magnetic force. The gel was allowed to swell until the equilibrium (l = 18.1mm and d = 410μm) in water under the load of the metal sphere before the application of the magnetic force. When DC is applied to the electromagnet at t = 0, the length l increases (Figure 2-3a) and the diameter d decreases (Figure 2-3b) instantaneously (l = 19.5mm and d = 393μm). This must correspond to the usual elastic-deformation without swelling, because the value of Poisson's ratio in the instantaneous deformation was around 0.47, as will be shown later. As can be seen from the figure, however,

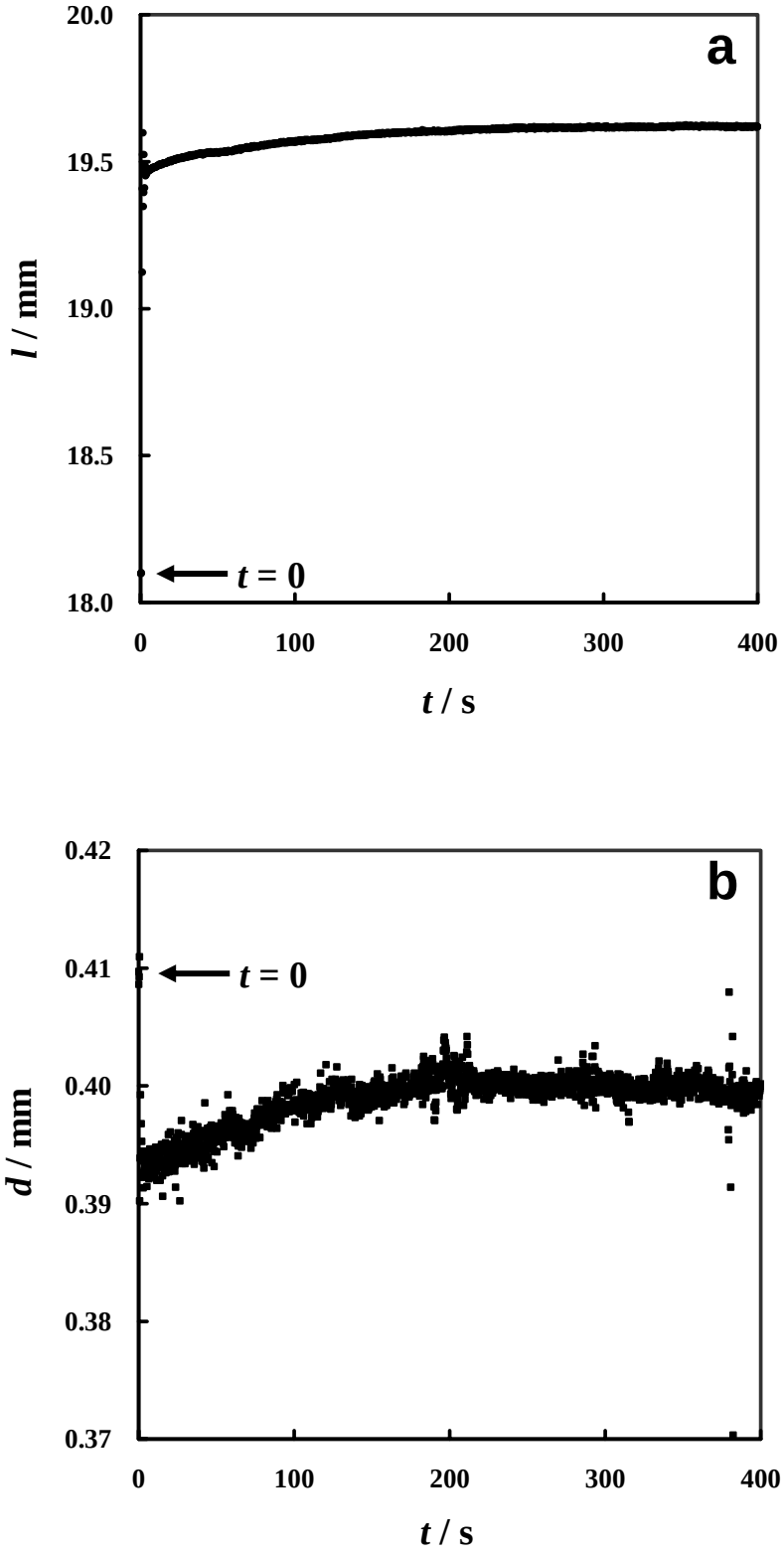

Figure 2-3 Time (*t*) dependence of (a) length *l* and (b) diameter *d* of the PNIPA gel in water after the imposition of the magnetic force.

l and d gradually increase in the region of t up to about 200s. These dimensional changes with t indicate that the stress-induced swelling occurs for the gel in water, because the increases in d and l evidently result in volume increase. Figure 2-4 shows the semi-logarithmic plots of l and d against t where l_0 and l_∞ represent l at t = +0 (just after deformation) and $t \rightarrow \infty$, respectively. The quantities d_0 and d_∞ also have the same meanings as l_0 and l_∞. In both plots, the data points appear to fall on a straight line, indicating the t-dependence is approximated to be single-exponential for the length as well as the diameter. A relaxation time for the stress-induced swelling (τ) is evaluated from the slope of each line: $\tau \approx$ 85s for the length; $\tau \approx$ 70s for the diameter. The values of τ for the length and diameter should be considered identical in view of the experimental error in estimating τ, and thus the relaxation time in both directions is evaluated to be about 80s.

A theory[9, 13] predicts that the diffusion constants in the radial and axial directions differ for infinitely long cylindrical gels: The change in diameter by stress-induced swelling is governed by the longitudinal mode while the change in length being by the transversal mode. On the basis of the theory, the ratio of the two diffusion constants (D_L/D_T), i.e, the ratio of the relaxation times for the swelling in the two directions, is given by $D_L/D_T = 2(1- \mu_\infty) / (1-2 \mu_\infty)$, where μ_∞ is the equilibrium Poisson ratio.[9, 13] As will be shown later, the gel samples used in this study show μ_∞=1/5~1/4, giving the ratio D_L/D_T of 8/3~3. This indicates that the two modes of relaxations are distinguishable in principle. The relaxation times for l and d in the present experiments were identical within experimental error. The reason for the disagreement of the theoretical prediction and the experimental results is unclear at present. The aspect ratio in the present

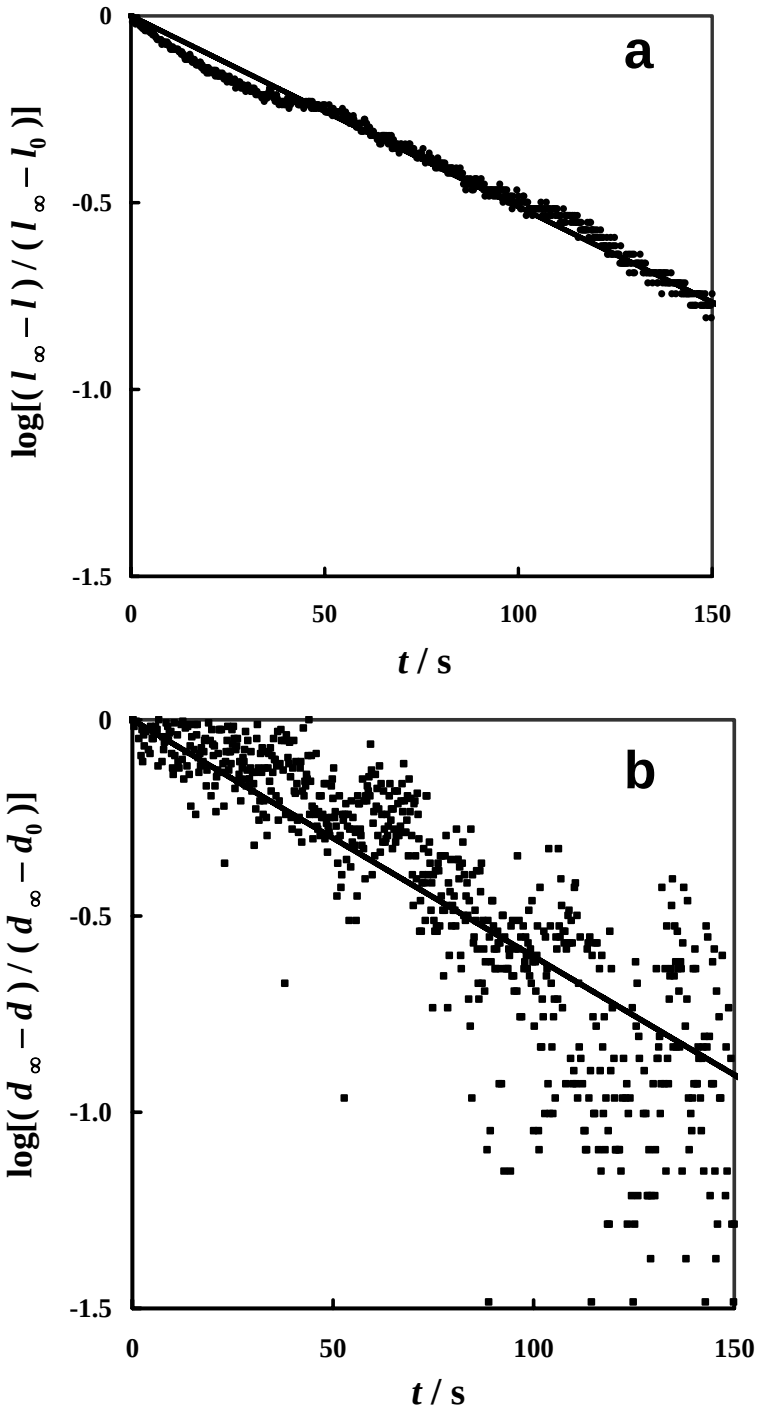

Figure 2-4 Semi-logarithmic plots for (a) $(l_\infty - l) / (l_\infty - l_0)$ and (b) $(d_\infty - d) / (d_\infty - d_0)$ as a function of time (t) where, l_0 and l_∞ represent l at $t = +0$ (just after deformation) and $t \to \infty$ in Figure 2-3, respectively. The quantities d_0 and d_∞ also have the same meanings as l_0 and l_∞. The straight lines represent approximation of single-exponential.

experiments ($l_0/d_0 \approx 30$) may still be insufficient to satisfy the condition of the infinite aspect ratio assumed in the theory. The theory does not give what value of aspect ratio is needed to observe the anisotropic swelling process. Further experiments using the gels with larger aspect ratios are needed to settle this issue.

In Figure 2-5 μ is plotted against t for the PNIPA gel in water. In this plot μ was defined by $\mu = -\Delta\varepsilon_\perp / \Delta\varepsilon_{//}$ with $\Delta\varepsilon_\perp = \varepsilon_\perp(t) - \varepsilon_\perp(t = -0)$ and $\Delta\varepsilon_{//} = \varepsilon_{//}(t) - \varepsilon_{//}(t = -0)$. The time at $t = -0$ stands for the time just before elongation by the magnetic force. This definition is a little different from the conventional one, but μ in the above definition is known to give the same value as from the conventional one as long as the deformation is small. Actually, the strains parallel to elongation in the present experiment never exceeded 20%, satisfying the condition of small deformation. At $t \approx 0$ μ lies around 0.47, and then μ decreases with increasing t. The value of μ at short times corresponds to the Poisson ratio as a material constant without swelling. The curve levels off at $t \approx$ 200s and the leveled-off value corresponding to the equilibrium Poisson ratio is estimated to be ca. 0.2, clearly indicating that stress-induced swelling occurs in the gel in water and the time profile of μ is almost the same as those of l and d (Figure 2-3).

2.4.2 Dynamic Properties

Figure 2-6 shows the plots of dynamic strain amplitudes ($\varepsilon_{//,0}$ and $\varepsilon_{\perp,0}$) against ω for the PNIPA gel in W and LP. For the gel in LP behaving as a soft elastic body like a rubber, both $\varepsilon_{//,0}$ and $\varepsilon_{\perp,0}$ are independent of ω. For the gel in W, however, a finite ω-dependence is observed in both $\varepsilon_{//,0}$ and $\varepsilon_{\perp,0}$; $\varepsilon_{//,0}$

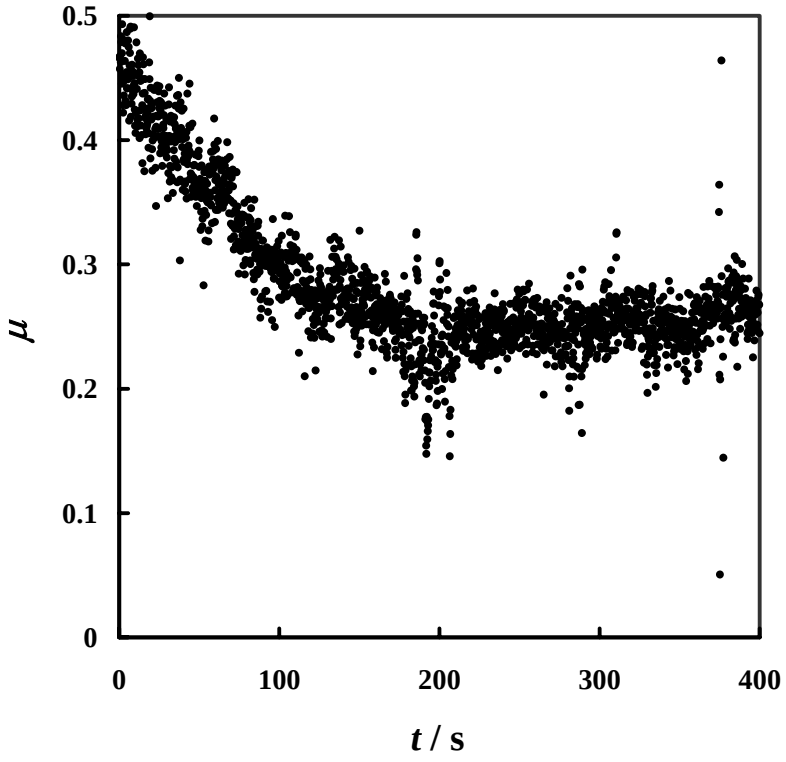

Figure 2-5 Time (t) dependence of Poisson's ratio (μ) obtained from the static test where $\mu = -\Delta\varepsilon_{\perp} / \Delta\varepsilon_{//}$ with $\Delta\varepsilon_{\perp} = \varepsilon_{\perp}(t) - \varepsilon_{\perp}(t = -0)$ and $\Delta\varepsilon_{//} = \varepsilon_{//}(t) - \varepsilon_{//}(t = -0)$. The time at $t = -0$ stands for the time just before elongation by the magnetic force in Figure 2-3.

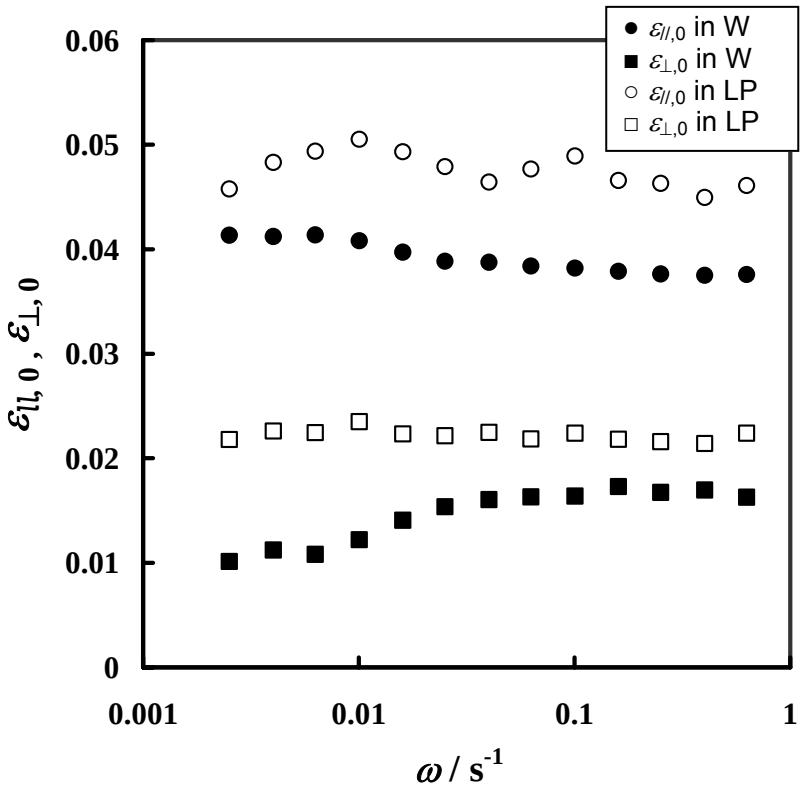

Figure 2-6 Angular frequency (ω) dependence of the dynamic strain amplitudes $\varepsilon_{//,0}$ and $\varepsilon_{\perp,0}$ for the PNIPA gel in water (●; $\varepsilon_{//,0}$: ■ ; $\varepsilon_{\perp,0}$) and in liquid paraffin (○ ; $\varepsilon_{//,0}$: □ ; $\varepsilon_{\perp,0}$).

increases and $\varepsilon_{\perp,0}$ decreases with decreasing ω. Using $\varepsilon_{//,0}$ and $\varepsilon_{\perp,0}$, we can calculate the absolute value of the dynamic Poisson ratio ($|\mu_D|$). In Figure 2-7 $|\mu_D|$ is plotted against ω for the gel in W and LP. No stress-induced swelling occurs for the gel in LP in the entire range of ω because the constant value estimated is ca. 0.47, close to 0.5, which agrees well with the value obtained from the static experiments in the short time limit. On the other hand, $|\mu_D|$ of the gel in W is strongly ω-dependent. At high frequencies at $\omega > 0.1s^{-1}$, $|\mu_D|$ is close to 0.5 similarly to μ in LP because the time scale for the sinusoidal force (ω^{-1}) is sufficiently shorter than the characteristic time for stress-induced swelling (τ), i.e., no occurrence of the stress-induced swelling. At frequencies at $\omega < 0.1s^{-1}$ where ω^{-1} is comparable to τ, the ω-dependence of $|\mu_D|$ becomes pronounced due to the emergence of the stress-induced swelling effect. The stress-induced swelling is equilibrated throughout the oscillation at low ω ($< 0.01s^{-1}$) where ω^{-1} is much longer than τ, with the result that $|\mu_D|$ shows level-off. The leveled-off value of $|\mu_D|$ at low ω lies about 0.25, which is rather close to the value of μ ($\mu \approx 0.2$) obtained by the static measurements in the long time limit (Figure 2-5).

Figure 2-8 shows the loss tangent of the phase lags ($\tan\delta_{//}$ and $\tan\delta_{\perp}$) as a function of ω. In LP, both of the loss tangents are almost the same and are constant independently of ω, lying around –0.1. This non-zero value indicates that the gel is viscoelastic, and $\varepsilon_{//,D}$ and $\varepsilon_{\perp,D}$ move with t by keeping $|\delta_{\perp} - \delta_{//}| = 0$. The PNIPA gel in W, on the other hand, shows a maximum on the $\tan\delta_{//}$ vs. ω plot and a minimum on the $\tan\delta_{\perp}$ vs. ω plots, reflecting the re-swelling by the applied force. The value of ω for the maximum is very close to that for the minimum. As stated Section 2.2, the dynamic Poisson ratio can be decomposed

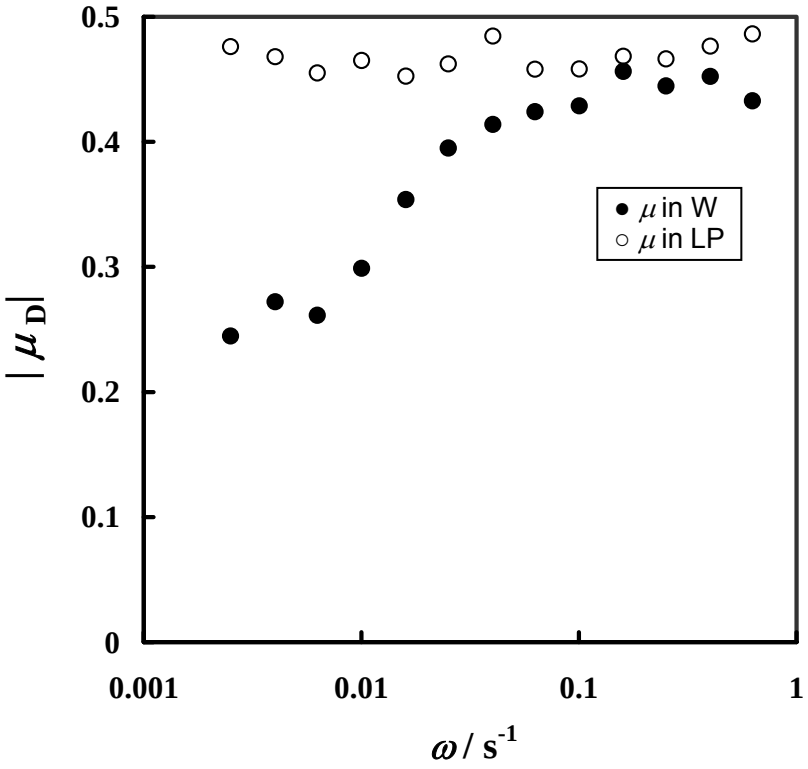

Figure 2-7 Angular frequency (ω) dependence of the absolute value of the dynamic Poisson ratio ($|\mu_D| = \varepsilon_{\perp,0} / \varepsilon_{//,0}$) for the gel in water (●) and in liquid paraffin (○).

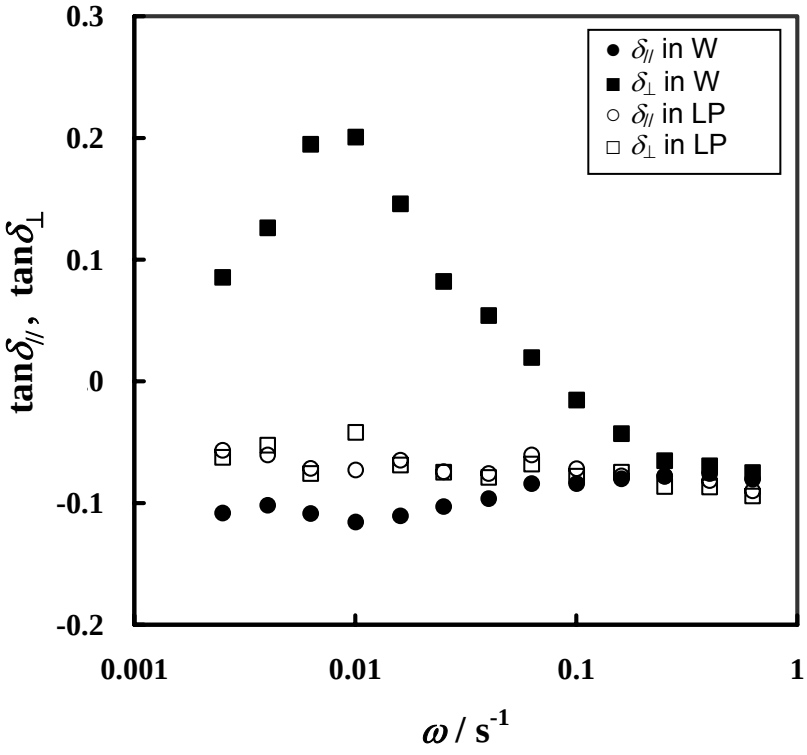

Figure 2-8 Angular frequency (ω) dependence of the loss tangent of the phase lags tan$\delta_{//}$ and tan $\delta_{\perp}$ in water (●; tan$\delta_{//}$: ■; tan $\delta_{\perp}$) and in liquid paraffin (○; tan$\delta_{//}$: □; tan $\delta_{\perp}$). The values $\delta_{//}$ and $\delta_{\perp}$ are the phase lags of $\varepsilon_{//,D}$ and $\varepsilon_{\perp,D}$ seeing from the stress wave, respectively.

into in-phase part μ_D' and the out-phase part μ_D". From Equation (2.8), μ_D' and μ_D" in W were calculated with the values shown in Figures 2.7 and 2.8. Figure 2-9 shows the Cole-Cole plot of the complex Poisson's ratio. The curve in the figure stands for a half circle and the data points appear to fall on the curve, indicating that μ_D relaxes almost in a single mode of the Debye-type.

A characteristic time for swelling in the dynamic tests is defined as the inverse of ω at the maximum (equivalently, at the minimum), and is evaluated to be around 100s both for the tan $\delta_\perp$ and tan $\delta_{//}$ curves (Figure 2-8). The value is also close to the τ determined by the static tests (ca. 80s). The agreement ensures the accuracy as well as reliability of the dynamic measurements. We would like to emphasize again that the relaxation observed stems from swelling, not from mechanical relaxation. This is also confirmed from the fact that τ is proportional to the square of the dimension of gels. A separate similar experiment shows $\tau \approx$ 180 s for the gel with the larger initial diameter (d^0 = 0.54 mm). The ratio of τ (180/100) for the two gels is close to the square of the ratio of d^0 ($(0.54/0.42)^2 \approx$ 1.7). It should be noticed that in the case of mechanical relaxation, the relaxation time is independent of the sample dimensions.

2.5 Conclusions

The effects of static and dynamic loading on the swelling properties of PNIPA hydrogels in the swollen state have been investigated by using a laboratory-made magnetic force-driven rheometer. In static tests (under a constant stress), the length and diameter of the cylindrical gel sample in water increase with time due to stress-induced swelling. Relaxation times of the

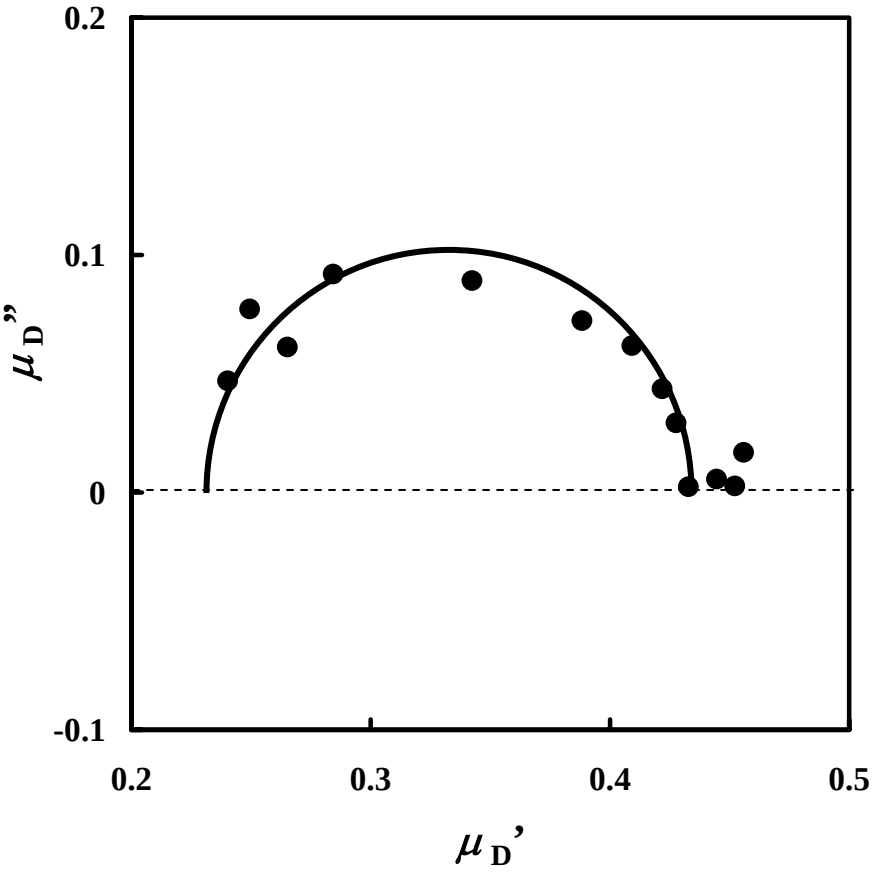

Figure 2-9 A Cole-Cole plot for μ_D for the PNIPA hydrogel.

stress-induced swelling in both directions are identical within experimental error. The Poisson ratio decreases from around 0.5 to around 0.2 with time just after the application of the magnetic force. The dynamic tests (under sinusoidal forces) reveal large differences in the swelling behavior of the gels surrounded with water and liquid paraffin (non-solvent for PNIPA gels). In liquid paraffin, amplitudes of strains parallel and perpendicular to elongation ($\varepsilon_{//,0}$ and $\varepsilon_{\perp,0}$, respectively) are independent of angular frequency (ω), giving the absolute value of dynamic Poisson ratio ($|\mu_D| = \varepsilon_{\perp,0} / \varepsilon_{//,0}$) of ca. 0.47. On the other hand, $\varepsilon_{//,0}$, $\varepsilon_{\perp,0}$ and $|\mu_D|$ in water significantly depend on ω due to the stress-induced swelling with a characteristic time. The dynamic Poisson ratio at $\omega \to \infty$ (short time limit) or $\omega \to 0$ (long time limit) agrees well with the corresponding Poisson's ratio obtained by the static tests. The phase lags of $\varepsilon_{//,D}$ and $\varepsilon_{\perp,D}$ seeing from the stress wave ($\delta_{//}$ and $\delta_{\perp}$, respectively) are independent of ω in liquid paraffin whereas $\varepsilon_{//,D}$ and $\varepsilon_{\perp,D}$ move with keeping $|\delta_{\perp} - \delta_{//}| = 0$. In water, the $\delta_{//}$ curve shows a minimum while the $\delta_{\perp}$ curve does a maximum at the same angular frequency. A characteristic time of swelling in the dynamic tests obtained as an inverse of this frequency accords well with the relaxation time in the static tests. It is also revealed that the dynamic Poisson ratio relaxes in a single mode of the Debye-type.

References

1. M. Shibayama, and T. Tanaka, *Adv. Polym. Sci.*, **109**, 1 (1993)
2. A. Khokhlov, S. Starodubtzev, and V. V. Vasilevskaya, *Adv. Polym. Sci.*, **109**, 123 (1993)
3. S. Hirotsu, *Adv. Polym. Sci.*, **110**, 1 (1993)
4. M. Doi, in "*Dynamics and Patterns in Complex Fluids*", A. Onuki and K. Kawaski ed., Springer, Berlin and Heidelberg, 1990
5. A. Suzuki, *Adv. Polym. Sci.*, **110**, 199 (1993)
6. T. Takigawa, T. Ikeda, Y. Takakura, and T. Masuda, *J. Chem. Phys.*, **117**, 7306 (2002)
7. S. Sasaki, and S. Koga, *Macromolecules*, **35**, 857 (2002)
8. S. Hirotsu, *Macromolecules*, **37**, 3415 (2004)
9. T. Takigawa, K. Urayama, Y. Morino, and T. Masuda, *Polymer Journal*, **25**, 929 (1993)
10. T. Takigawa, K. Uchida, K. Takahashi, and T. Masuda, *J. Chem. Phys.*, **111**, 2295 (1999)
11. T. Tanaka, and D. J. Fillmore, *J. Chem. Phys.*, **70**, 1214 (1979)
12. L. D. Landau and E. M. Lifshitz, "*Theory of Elasticity*", Pergamon Press, Oxford, 1986
13. T. Takigawa, K. Urayama, and T. Masuda, *Polymer Gels and Networks*, **2**, 59 (1994)

Chapter 3

Effects of Static and Dynamic Loading on Swelling of Poly(*N*-isopropylacrylamide) Gels in the Collapsed State

3.1 Introduction

The volume of polymer gels varies in response to the change in the environmental factors such as temperature, pH, composition of the solvent.[1-4] As described in Chapter 1, it is well known that poly(*N*-isopropylacrylamide) (PNIPA) hydrogels undergo the volume phase transition at the transition temperature (T_t): Below T_t the gels are in "the swollen state" while above T_t in "the collapsed state". In Chapter 2, we investigated the swelling behavior of the PNIPA hydrogels in the swollen state below T_t under static or dynamic loading. We observed a pronounced "stress-induced swelling".[5,6] By contrast, there are few corresponding measurements on the PNIPA gels in the collapsed state above T_t and thus the details of the deformation behavior of the collapsed gels are still unclear.[7-9] In this chapter, we describe the deformation behavior of the collapsed PNIPA gels under static and dynamic stresses (or strains) revealed by the same method in Chapter 2.

3.2 Experimental

3.2.1 Materials

Poly(*N*-isopropylacrylamide) (PNIPA) hydrogels were synthesized by the same method in Chapter 2, namely the radical copolymerization of NIPA and BIS. The total monomer concentration of NIPA and BIS was fixed to be 6 wt%,

and the molar ratio [NIPA] / [BIS] was also fixed to be 100. The concentrations of AP (initiator) and TEMED (accelerator) were 0.8 g/l and 2.4 ml/l, respectively. The obtained cylindrical gel samples were then removed from the capillaries and were poured into a large amount of methanol at room temperature to exchange the solvent from water to methanol. The methanol outside the gels was exchanged at several times. The gels swollen by methanol were dried *in vacuo*, and thenafter they were soaked in water at about 50 °C to obtain the samples in the equilibrium collapsed state. The dimensions of the samples used for mechanical tests were 10-20 mm in length and 0.5-2.0 mm in diameter.

3.2.2 Measurements

The same apparatus shown in Chapter 2 was used to examine all the measurements. In this study, we carried out the strain-controlled operations in addition to the same measurements (stress-controlled operation) as described in Chapter 2, so that some details of the apparatus were illustrated in Figure 3-1.

In strain-controlled operations, one end of the gels was settled with a larger, hence heavier, metal sphere; in this condition, the gel is elongated by about 50 %, and the metal sphere touches on the bottom of the bath. As a result, the strain in the stretching direction is fixed throughout the measurement. The length of the gels was fixed to be a constant value and was estimated by the height of the moving plate from the bottom, while the change in diameter was determined by using a set of emitter-detector unit. In this operation, liquid paraffin (LP) as well as water (W) was employed as the surrounding solvent of the fully swollen gel by water. LP is a non-solvent for PNIPA. Temperature-controlled water was circulated in the outer bath at around 40°C

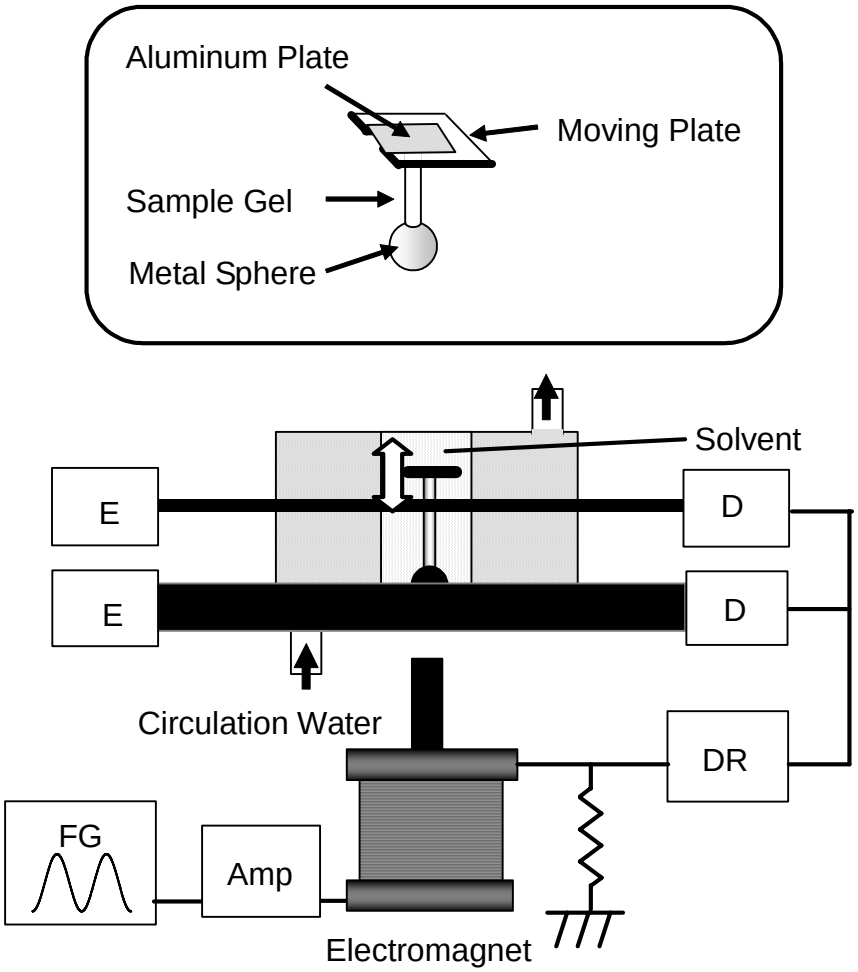

Figure 3-1 The schematic representaion of the magnetic force-driven rheometer. FG; function generator: Amp; power amplifier: E; emitter part of laser scan micrometer: D; detector of laser scan micrometer: DR; Digital Recorder.

(above T_t) throughout this study.

3.3 Results and Discussion

3.3.1 Static Properties

Figure 3-2 show the *t*-dependence of the length (*l*) and diameter (*d*) after the application of the static stress to the collapsed PNIPA gel in water. In this measurement the maximum strain in the axial direction is ca. 3% which is within linear elasticity region. The length *l* increases (Figure 3-2a) and the diameter *d* decreases (Figure 3-2b) with increasing time, and these reach the equilibrium values at about t = 600 s. This behavior is actually a kind of creep, and is substantially different from the behavior of the PNIPA gels in the swollen state shown in Chapter 2 (Figure 2-3): Both length and diameter increased under a constant stress, namely, the gels in the swollen state clearly showed the further swelling induced by the static stress. The different behavior of the collapsed and swollen PNIPA gels under a constant stress probably results from the difference in cross-links. The collapsed PNIPA gels have the cross-links formed by hydrogen bonds in addition to the cross-links made of covalent bonds owing to the high network density.[7] The network concentration of the collapsed gel is about eight times as large as that in the swollen state. In contrast the swollen gels were made only of the covalent bonds. When the mechanical stress is applied to the collapsed gel, the hydrogen bonds are destroyed instantaneously by the stress. But all hydrogen bonds are not destroyed at once. Only the hydrogen bonds which directly supports the force are destroyed. In addition, new hydrogen bonds are generated in other places at the same moment because the some network chains come close each other by the deformation. Through the

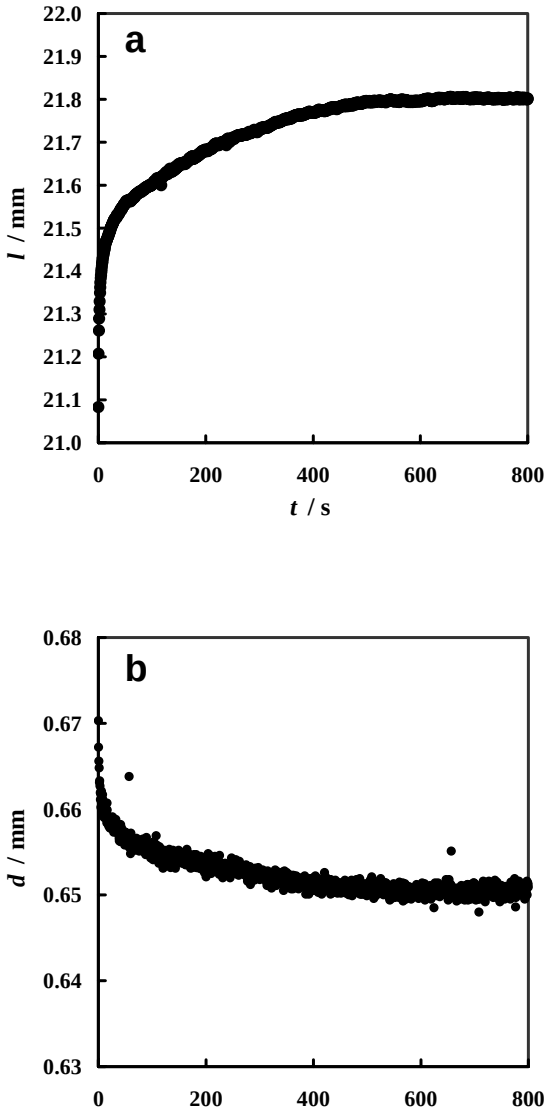

Figure 3-2 Time dependence of (a) the length (*l*) and (b) the diameter (*d*) of the PNIPA hydrogel in the collapsed state after applying the a static stress (the voltage of the applied DC is 4V).

deformation of the gel, the network repeats the generation as well as destruction, namely the recombination, of the hydrogen bonds. This causes the slow creep behavior of the collapsed gel. When the elastic force of the network balances with the applied stress, the recombination of the hydrogen bonds ceases.

Figure 3-3 shows the *t*-dependence of *l* and *d* for the collapsed gel in water after the applied stress is removed. The length decreases (Figure 3-3a) and the diameter increases (Figure 3-3b) with increasing elapsed time. At about t = 600 s the gel reaches the equilibrium state, which is very close to the original state before deformation. This corresponds to the process of creep recovery. After the removal of the applied stress, the creep recovery proceeds via the reverse process of the recombination of the hydrogen bonds.

The Figure 3-4a shows the *t*-dependence of *d* after applying the static strain in water. The applied strain is about 50 % and the inset shows the result for the small strain of about 5 %. The initial diameter before deformation was 2.4 mm. The static strain induces a finite further swelling. The stress-induced swelling becomes more clearly recognizable as the strain increases. In the case of 50% strain, the diameter levels off at about 150 s. The results of the static strain experiments confirm that the stress-induced swelling occurs even in the collapsed state although the magnitude is smaller than that in the swollen state. The stress-induced swelling was not recognizable in the variation of *d* in the constant stress experiment (Figure 3-2). This is probably because the increasing in *d* by the stress-induced swelling is effectively masked by the decrease in *d* caused by the creep. Figure 3-4b displays the results of the similar experiments in LP (non-solvent for PNIPA). The diameter of the gel shows no appreciable change over the whole range of *t*. These results further confirm that the variation

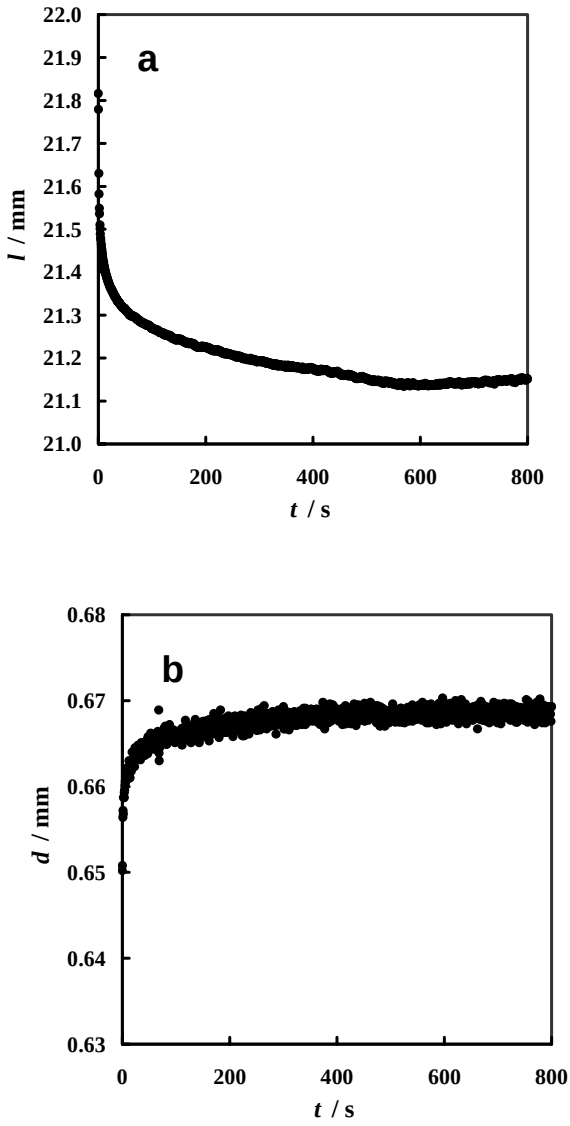

Figure 3-3 Time course of (a) the length (*l*) and (b) the diameter (*d*) of the gel after releasing the applied stress.

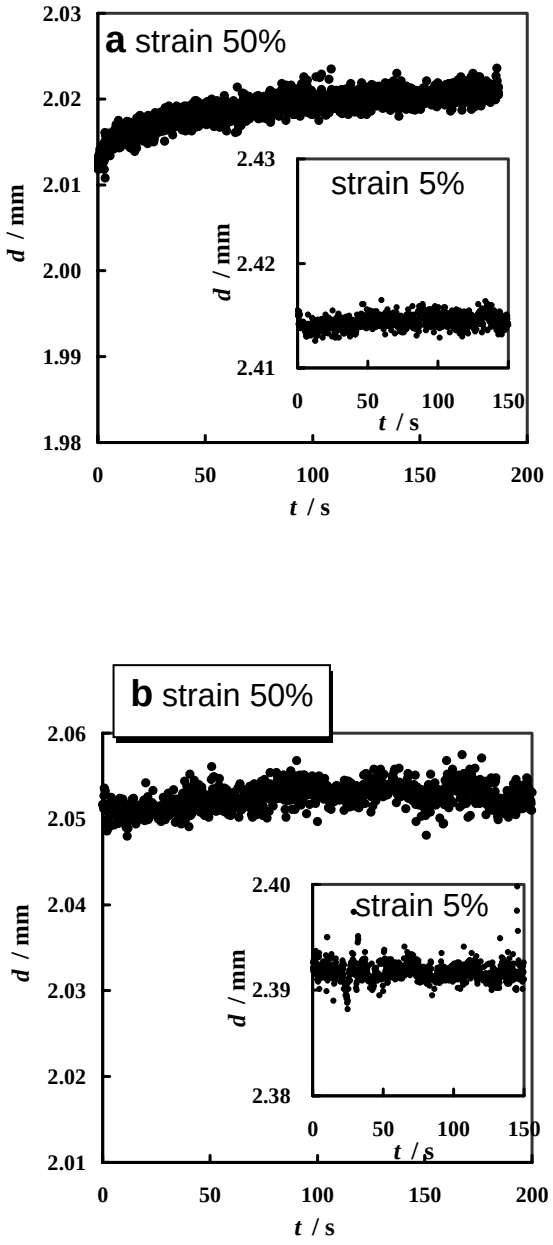

Figure 3-4 Time dependence of the diameter (*d*) of gel under 50% strain in (a) water and (b) LP. The each inset is same value of 5% strain.

of *d* in water (Figure 3-4a) are attributed to the stress-induced swelling.

3.3.2 Dynamic Properties

In order to analyze the dynamic data, the definitions of the dynamic variables in Chapter 2 were employed. In this chapter, we employ the dynamic change in length Δl_D instead of the dynamic strain as a variable for our convenience. We define the variation of length for the gel in the dynamic measurements (Δl_D) as

$$\Delta l_D = \Delta l \exp[i(\omega t - \delta)] \qquad (3.1)$$

where Δl, and δ represent the amplitude of the displacement and the phase lag (seen from the stress), respectively. Note that the phase lag δ defined by Equation (3.1) is opposite in the sign in the definition in Chapter 2 (Equation (2.5a), namely the range of δ is defined as $0 \le \delta \le \pi / 2$ for viscoelastic bodies.

Figure 3-5 shows the semi-logarithmic plots of Δl and δ against ω for the PNIPA hydrogel in the collapsed state. The amplitude Δl decreases monotonically with increasing ω and the value of Δl at the lowest frequency is about five times as large as that at the highest frequency. This result is significantly quite different from the results for the PNIPA gels in the swollen state in Chapter 2 (Figure 2-6), where the two plateau regions emerge in the low and high frequency limit. Figure 3-5b shows the plots for δ. The phase lag increases with increasing ω, and at high frequencies δ increases very steeply. This behavior is also different from that in the swollen state (Figure 2-8). The dynamic valuable Δl_D can be decomposed into the in-phase part ($\Delta l_D'$) and the out-of-phase part ($\Delta l_D''$). Each can be written by

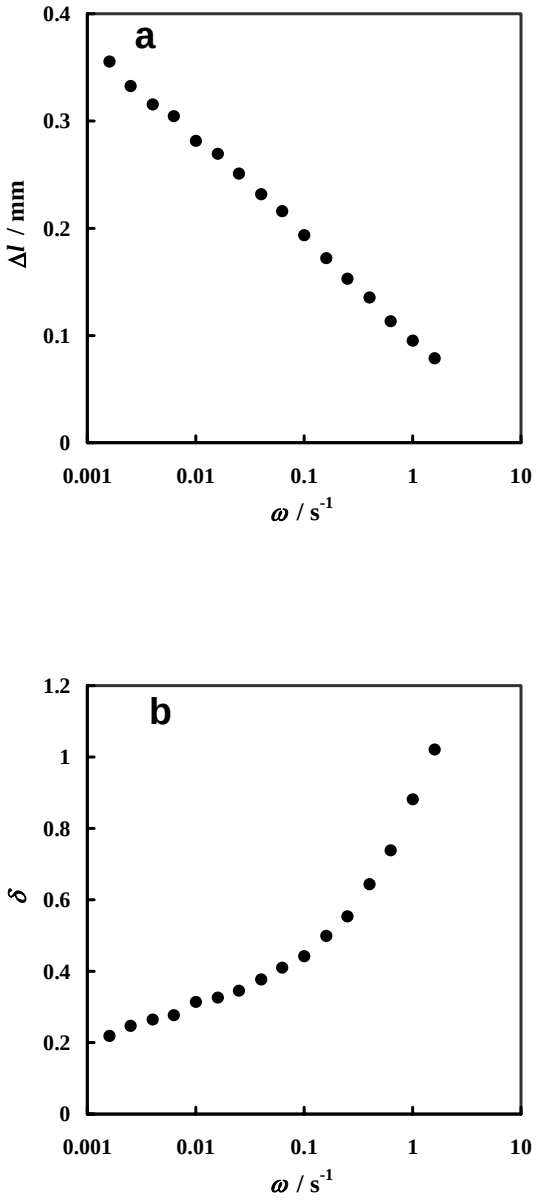

Figure 3-5 (a) Amplitude of the displacement induced (Δl) by the dynamic stress as a function of angular frequency (ω), and (b) phase lag (δ) determined as a function of angular frequency (ω) (the amplitude of the applied AC voltage is 2V).

$$\Delta l'_{\mathrm{D}} = \Delta l \cos\delta \tag{3.2a}$$

$$\Delta l''_{\mathrm{D}} = \Delta l \sin\delta \tag{3.2b}$$

Figure 3-6 shows the ω-dependence of $\Delta l_{\mathrm{D}}'$ and $\Delta l_{\mathrm{D}}''$ (circles and squares, respectively) of the PNIPA gel. The in-phase part $\Delta l_{\mathrm{D}}'$ decreases with increasing ω as in the case of the Δl, whereas $\Delta l_{\mathrm{D}}''$ is almost constant over a wide range of ω. This indicates that the creep occurred with the same intensity in the whole ω-range examined because $\Delta l_{\mathrm{D}}''$ corresponds to the creep intensity.

3.3.3 Comparison between Static and Dynamic Data

In order to check the consistency between the static and dynamic data of the collapsed gels, we compare the experimental data obtained from static measurements with the static response calculated form the dynamic data. The gel specimen is the same for the static and dynamic tests (Figures 3-2 and 3-6, respectively). On basis of the almost ω-independent $\Delta l_{\mathrm{D}}''$, we assume the following spectrum.

$$\Delta l_D = k\sum_{n=1}^{m}\frac{1}{1+\mathrm{i}\,\omega\tau_n} \tag{3.3a}$$

where Δl_{D} is defined by

$$\Delta l_{\mathrm{D}} \equiv \Delta l'_{\mathrm{D}} - \mathrm{i}\,\Delta l''_{\mathrm{D}} \tag{3.3b}$$

The functions $\Delta l_{\mathrm{D}}'$ and $\Delta l_{\mathrm{D}}''$ from Equation (3.3a) satisfy the Kramers-Kronig relation.[10] The mechanism of the change in length is assumed to be of multi-mode, each being only virtual and not corresponding to the real mode of motion. In Equation (3.3a), k and τ_{n} are respectively the intensity and the retardation time of the n-th mode (n = 1, 2,...m). The distribution of τ_{n} in

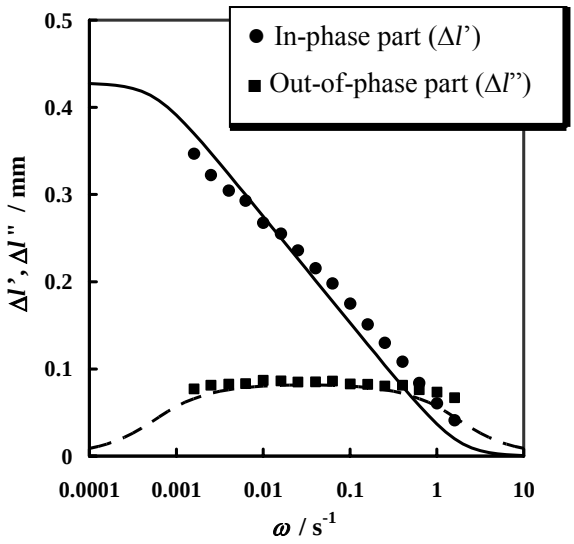

Figure 3-6 In-phase part ($\Delta l_D'$; ●) and out-of-phase part ($\Delta l_D''$; ■) of the amplitude of the displacement as a function of angular frequency (ω). The best fit curves of $\Delta l_D'$ and $\Delta l_D''$ also shown as a solid line and broken line (see text).

Equation (3.3a) is separated with the same time interval in a logarithmic scale. The cut-off value of τ in the long time limit is assumed as τ_1 = 1000 s. Although the edge in the lower frequency side of the box-shape spectrum was not observed in the dynamic test, but it is simply expected that τ_1 is not so far from the longest retardation time (ca. 200 s) directly obtained in the static experiment. The intensity k (= 0.061 mm) and the cut-off value of the short time limit (τ_7) were evaluated by the best fitting with m = 7 to the data of $\Delta l'$. The value of m (m = 7) is chosen so that Equation (3.3a) can reproduce the box-type spectrum, and the values of $m \geq 7$ yield the same results as m = 7. The fitting result is shown in Figure 3-6.

The variation of the length $\Delta l(t)$ is defined as $\Delta l(t) = l(t) - l_0$ with initial length l_0, and we have

$$\frac{\mathrm{d}}{\mathrm{d}t}\Delta l(t) = \frac{k}{2\pi}\sum_{n=1}^{7}\int_{-\infty}^{\infty}\frac{1}{1+\mathrm{i}\,\omega\tau_n}\exp(i\omega t)\mathrm{d}\,\omega = k\sum_{n=1}^{7}\frac{1}{\tau_n}\exp\left(-\frac{t}{\tau_n}\right) \qquad (3.4a)$$

Integration of the above equation over t with the initial condition for $\Delta l(t)$ gives

$$\Delta l(t) = k\sum_{n=1}^{7}\left[1-\exp\left(-\frac{t}{\tau_n}\right)\right] \qquad (3.4b)$$

Figure 3-7 compares the result of the static test (the data in Figure 3-2a) and the curve calculated from Equation (3.4b). The good agreement shows that the dynamic and static data are consistent. The fitted values of the initial length l_0 and k are 21.08 mm and 0.11 mm, respectively. This value of k is about twice as large as k = 0.061 mm for the fitting to the dynamic data. This is reasonable because the effective magnitude of the applied stress (voltage) in the static test (Figure 3-2) is two times larger than that in the dynamic test (Figure 3-5).

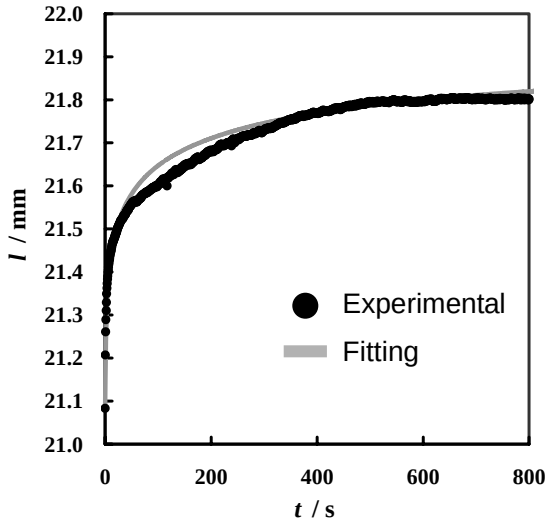

Figure 3-7 Time dependence of the length (l) (black circle) after applying the a static stress in Figure 3-2a and the best fit curve converted from dynamic date (gray line).

3.4 Conclusions

We investigated the deformation behavior of the PNIPA hydrogels in the collapsed state under static and dynamic stresses. When a constant stress was applied to the collapsed gels in water, the length increased and the diameter decreased toward the new equilibrium values. When the stress was released, the length and diameter recovered the original values before deformation. This creep and creep recovery originated from the destruction and generation of the hydrogen bonds in the collapsed gels. In the measurements under constant strains, a small but definite stress-induced swelling occurred. In the collapsed state the deformation after the stress imposition was dominated by the creep accompanying a small degree of stress-induced swelling, while in the swollen state the deformation was mainly governed by the stress-induced swelling.

In the dynamic measurements, the amplitude of the displacement in length decreased and the phase lag increased as angular frequency increases. The static properties obtained by the conversion of the dynamic data agreed with the static data in the experiment.

References

1. S. Hirotsu, *Adv. Polym. Sci.*, **110**, 1 (1993)
2. M. Shibayama, and T. Tanaka, *Adv. Polym. Sci.*, **109**, 1 (1993)
3. A. Khokhlov, S. Starodubtzev, and V. V. Vasilevskaya, *Adv. Polym. Sci.*, **109**, 123 (1993)
4. A. Suzuki, *Adv. Polym. Sci.*, **110**, 199 (1993)
5. T. Yamaue, and M. Doi, *Phys. Rev. E*, **69**, 041402 (2004)
6. T. Yamaue, and M. Doi, *Phys. Rev. E*, **70**, 011401 (2004)
7. T. Takigawa, T. Ikeda, Y. Takakura, and T. Masuda, *J. Chem. Phys.*, **117**, 7306 (2002)
8. S. Sasaki, and S. Koga, *Macromolecules*, **35**, 857 (2002)
9. S. Hirotsu, *Macromolecules*, **37**, 3415 (2004)
10. J. D. Ferry, "*Viscoelastic Properties of Polymers Third Edition*", Toronto, Brisbane, Chichester, New York (1980)

Chapter 4

Kinetics of Shrinking of Polyacrylamide Gels Induced by Ultracentrifugal Fields

4.1 Introduction

As described in Chapter 1, the kinetics of swelling and shrinking of polymer gels in solvents has been investigated from the experimental and theoretical viewpoints. The kinetics of polymer gels has been analyzed on the basis of diffusion models of networks.[1-6] On the basis of the diffusion models, the characteristic time for swelling and shrinking is of the order of d^2 / D, where d and D are the final dimension of the gel and the diffusion constant of the network, respectively. The constant D is governed by the elastic and frictional characteristics of networks as $D = L/f$ where L and f are the longitudinal elastic modulus and friction coefficient between network and solvent, respectively. The elastic moduli such as Young's modulus and shear modulus can be easily measured by conventional mechanical testing. By contrast, there exist only a few studies[1,8,9] on the measurements of f due to the limited experimental methods.

The dynamics of swelling and shrinking of gels has been investigated under no external field[1-4] as well as under static strains,[7,10-15] and dynamic load in Chapters 2 and 3. In this chapter, we focuses on the shrinking behavior of gels under constant ultracentrifugal fields which has not been reported before. A theory based on the diffusion model is proposed to describe the kinetics of the

shrinking of gels driven by centrifugal fields. We also conduct the corresponding experiments, and the whole shrinking process observed is compared by the theoretical prediction. We examine the shrinking behavior of a polyacrylamide (PAAm) hydrogel and poly (vinyl alcohol) gel, each of which is classified into "chemical gel" and "physical gel", respectively. In this chapter, we focus on the former gel. The results of the latter gel will be described in the next chapter.

4.2 Theory

4.2.1 Basic Equations

In this section, we theoretically describe the kinetics of shrinking of a polymer network driven by a centrifugal field. The system considered here is illustrated in Figure 4-1. A gel (polymer network swollen in solvent) confined at the bottom of a cell is placed under a centrifugal field generated by angular velocity Ω. The center of rotation, the gel surface in the initial state and the bottom of the cell are designated at $r = 0$, $r = r_1$ and $r = r_2$, respectively, where the r-axis coincides with the direction of the centrifugal force. In the present condition, the deformation of the network takes place only in the r-direction because of the presence of the side walls of the cell, if we assume the slip boundary for the interface between the gel and side walls.

According to the diffusion model introduced by Tanaka et al.,[1] the equation of motion for a unit volume element in the network with density ρ_N under an external field is generally written as

$$\phi\rho_N \frac{\partial^2 \mathbf{u}}{\partial t^2} = \nabla \bullet \boldsymbol{\sigma} - f\frac{\partial \mathbf{u}}{\partial t} + \mathbf{F} \qquad (4.1)$$

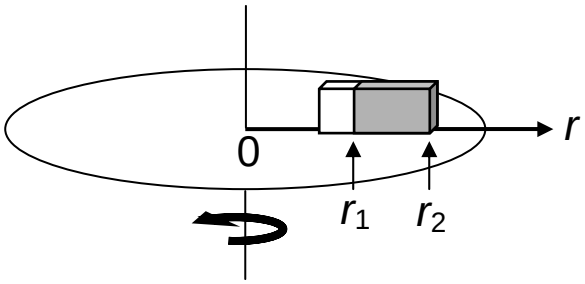

Figure 4-1 Schematic for a gel under centrifugal fields. The gray part indicates a gel confined in a cell. Each of r_1 and r_2 corresponds to the position of the moving boundary (gel surface) and immobile bottom wall of the cell.

where **u** is the displacement vector representing the displacement of a point from the initial position at $t = 0$, and ϕ is the volume fraction of the network. The vector **F** denotes the force resulting from the external field concerned. The term on the left hand side of the equation is safely neglected because the motion concerned is sufficiently slow. The terms on the right hand side represent the forces acting on the element. The first term is the gross force from the internal stresses, which is given by the divergence of the stress tensor $\boldsymbol{\sigma}$. According to the linear elasticity theory, in the rectangular coordinates (O-$x_1x_2x_3$), $\boldsymbol{\sigma}$ is related to **u** as[16]

$$\sigma_{ij} = \left(K - \frac{2}{3} G \right) \nabla \bullet \mathbf{u} \delta_{ij} + G \left(\frac{\partial u_i}{\partial x_j} + \frac{\partial u_j}{\partial x_i} \right) \tag{4.2}$$

where K and G are the osmotic bulk modulus and shear modulus of the network alone, respectively. The second term in Equation (4.1) is the frictional force expressed as a product of velocity of the element and friction coefficient f between network and solvent inside the gel. In the present study, the third term originates from a centrifugal field. The centrifugal force acting on the element at distance r from the origin is proportional to $r\Omega^2$ as well as the difference in density $\Delta\rho$ between polymer network and solvent.

The network is deformable only in the radial direction under the condition concerned. As a result, this shrinking behavior may be treated as one-dimensional (1D) diffusion of the network. From Equations (4.1) and (4.2) with neglecting the left-hand side term of Equation (4.1), we obtain the equation for $u(r, t)$:

$$\frac{\partial u(r,t)}{\partial t} = D \frac{\partial^2 u(r,t)}{\partial r^2} + \frac{\phi \Delta\rho \omega \Omega^2}{f} r \tag{4.3}$$

where $D = (K + 4G/3) / f = L / f$ is the diffusion constant of the network.

4.2.2 Solution

The initial condition to solve Equation (4.3) is given by

$$u(r, 0) = 0 \qquad \text{at } t = 0 \tag{4.4}$$

The boundary conditions at the surface ($r = r_1$) and bottom ($r = r_2$) of the cell may be respectively given by

$$\frac{\partial u(r_1, t)}{\partial r} = 0 \qquad \text{at } r = r_1 \tag{4.5}$$

and

$$u(r_2, t) = 0 \qquad \text{at } r = r_2 \tag{4.6}$$

Equation (4.5) originates from that the stress normally acting on the gel surface (moving surface) is zero.[2] The solution of Equation (4.3) satisfying the initial and boundary conditions is

$$u(r,t) = \sum_{n=1}^{\infty} A_n \exp\left(-\frac{(2n-1)^2 t}{\tau_L}\right) + u(r,\infty) \tag{4.7a}$$

with

$$A_n(r) = \frac{16a^2\phi\Delta\rho\Omega^2}{\pi^4 L}\left\{\frac{(-1)^n \pi r_2}{(2n-1)^3} + \frac{2a}{(2n-1)^4}\right\}\cos\left\{\frac{(2n-1)\pi(r-r_1)}{2a}\right\} \tag{4.7b}$$

where $a = r_2 - r_1$. In Equation (4.7a), τ_L is the longest characteristic time defined by

$$\tau_L = \frac{4a^2}{\pi^2 D} \tag{4.8}$$

The term $u(r,\infty)$ in Equation (4.7a) is the stationary value of u in the long time limit:

$$u(r,\infty) = \frac{\phi\Delta\rho\Omega^2}{6L}\left(r_2^{\,3} + 3r_1^{\,2}r - 3r_1^{\,2}r_2 - r^3\right) \tag{4.9}$$

In particular, the displacement of the moving surface in the stationary state $u(r_1,\infty)$ is given by

$$u(r_1,\infty) = \frac{\phi\Delta\rho\Omega^2}{6L}\left(2r_1^{\,3} - 3r_1^{\,2}r_2 + r_2^{\,3}\right) \tag{4.10}$$

Equations (4.9) and (4.10) indicate that the shrinkage in the steady state is determined by the balance between the centrifugal force and the elastic force. Meanwhile, in the initial stage of shrinking at $t/\tau_L \ll 1$, $u(r_1,t)$ given by Equation (4.7) with $r = r_1$ is approximated to be the linear function of t as

$$u(r_1,t) = \frac{\phi\Delta\rho r_1\Omega^2}{f}t \qquad \text{for } t/\tau_L \ll 1 \tag{4.11a}$$

or

$$v(r_1,t) \equiv \frac{d}{dt}u(r_1,t) = \frac{\phi\Delta\rho r_1\Omega^2}{f} \tag{4.11b}$$

with using the shrinking velocity v. Equation (4.11) shows that the initial shrinking rate is proportional to the ratio of the centrifugal force to the frictional force. Thus the shrinking behavior in the short or long time limit strongly reflects the frictional or elastic property of gels, respectively.

Figure 4-2 illustrates $u(r,t)/u(r_1,\infty)$ as a function of r/r_2 at various reduced times t/τ_L, i.e., the displacement distribution of a gel during shrinking. In the calculation, $r_1 = 6 \times 10^{-2}$ m and $r_2 = 7 \times 10^{-2}$ m, both of which are close to the experimental condition in present study, were employed. In the initial state $t = 0$, $u(r,0) = 0$. The profile of the stationary displacement is given by a cubic function of r of Equation (4.9).

Figure 4-3 displays the displacement of the moving surface $u(r_1,t)$ at various centrifugal accelerations α ($=r_1\Omega^2/g$ where g is the acceleration of

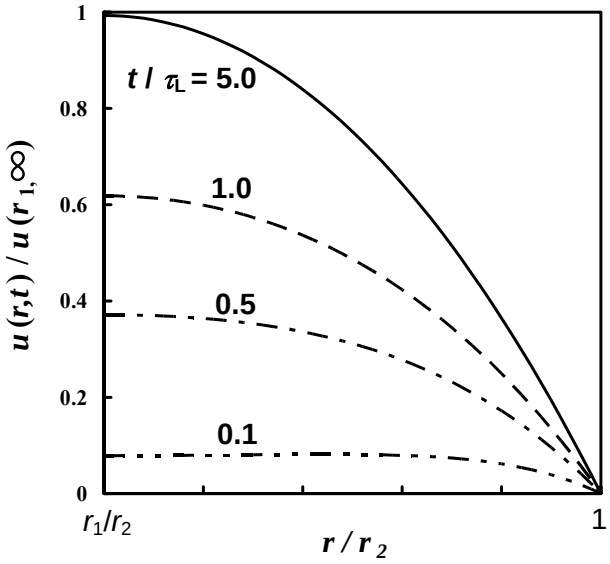

Figure 4-2 The displacement distribution of a gel during shrinking. The relative position $u(r,t)/u(r_1,\infty)$ is displayed as a function of r/r_2 at various reduced time t / τ_L. In the calculation, $r_1 = 6 \times 10^{-2}$ m and $r_2 = 7 \times 10^{-2}$ m are employed.

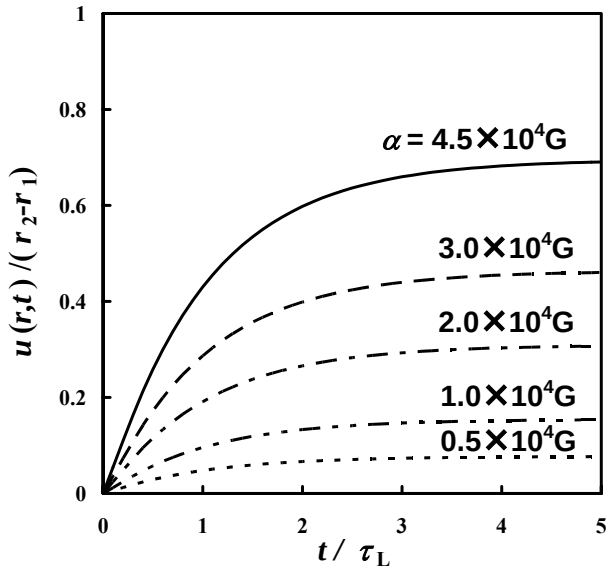

Figure 4-3 The shrinking behavior of a gel at various centrifugal accelerations (α). The calculation is performed with $r_1 = 6 \times 10^{-2}$ m, $r_2 = 7 \times 10^{-2}$ m, $L = 3 \times 10^4$ Pa, $f = 1 \times 10^{14}$ Ns/m^4, $\phi = 2 \times 10^{-2}$, $\Delta\rho = 4.48 \times 10^2$ kg/m^3.

gravity) as a function of reduced time t/τ_L. The calculation was performed with $r_1 = 6 \times 10^{-2}$ m, $r_2 = 7 \times 10^{-2}$ m, $L = 3 \times 10^4$ Pa, $f = 1 \times 10^{14}$ Ns/m^4, $\phi = 2 \times 10^{-2}$ and $\Delta\rho = 4.48 \times 10^2$ kg/m^3. As α increases, each of the initial shrinking rate and the stationary shrinkage increases as expected from Equations (4.10) and (4.11), respectively.

Although the exact solution of $u(r,t)$ is a multiexponential function shown by Equation (4.7), the solution is well approximated by a single exponential function just with the leading term for n=1: The contributions of the high-order terms ($n \geq 2$) proportional to $1/(2n\text{-}1)^3$ are negligibly small relative to that for n=1. Thus the expression of $u(r_1,t)$ is reasonably simplified as

$$u(r_1,t) \approx \frac{16a^2}{\pi^4}\frac{\phi\Delta\rho\Omega^2}{L}(2a-\pi r_2)\exp\left(-\frac{t}{\tau_L}\right)+u(r_1,\infty) \qquad (4.12)$$

It is seen in Figure 4-4 that there exists no noticeable difference in the whole time dependence of $u(r_1, t)$ given by Equation (4.7) and Equation (4.12).

In this study, we actually observe the concentration gradient in the cell from the Schlieren patterns during the measurement. that the concentration (c) of the polymer network is briefly explained. Since the shrinking of the gel is supposed to be one-dimensional deformation, the concentration of the polymer network normalized initial concentration c_0 is written with the displacement $u(r, t)$ as

$$\frac{c(r,t)}{c_0} = \frac{1}{1+\dfrac{\partial u(r,t)}{\partial r}} \qquad (4.13)$$

Thus the concentration gradient is written in the following form.

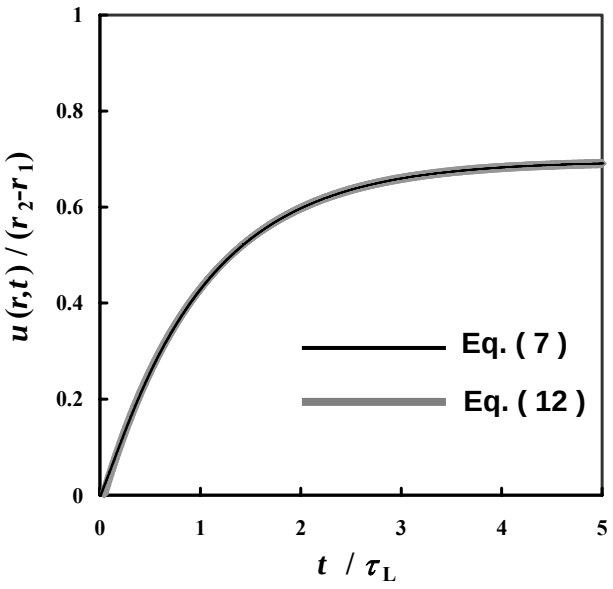

Figure 4-4 The comparison of $u(r,t)$ given by Equations (4.7) and (4.12). The former is calculated by summing the terms up to n=1000. No appreciable difference is present between the two curves over the whole time region. The curves are calculated with $\alpha = 4.5 \times 10^4$ G and the same parameter values as Figure 4-3.

$$\frac{\partial}{\partial r}\frac{c(r,t)}{c_0} = \frac{-\dfrac{\partial^2 u(r,t)}{\partial r^2}}{\left(1+\dfrac{\partial u(r,t)}{\partial r}\right)^2} \tag{4.14}$$

Figure 4-5 shows the plots of the calculated concentration gradient inside the gel various *t*. The gradient was calculated from Equation (4.14) and the movement of the gel itself is taken into account for the data. The centrifugal acceleration α = 4.5 × 10^4 G and the same parameters as Figure 4-3 were employed for the calculation. As *t* increases the upturn near the bottom becomes pronounced. This indicates that the concentration of the polymer network near the bottom, where the movement of the gel is constrained, significantly increase by shrinking of the gel.

4.3 Experimental

4.3.1 Materials

Polyacrylamide (PAAm) gels were prepared by radical copolymerization of acrylamide monomer and methylenebisacrylamide (BIS) (crosslinker) employing ammoniumpersulfate as an initiator. The mixtures were dissolved in water. The monomer concentration was 3.00 wt%, and the molar ratio [PAAm] / [BIS] was 100. After the pregel solution was poured into an optical cell for the ultracentrifugal measurement, the cell was maintained at 5 ^{o}C for 24 hours for cross-linking reactions. The concentrations of AP (initiator) and TEMED (accelerator) were 0.8 g/l and 2.4 ml/l, respectively.

As the value of ρ_N for PAAm networks is unknown, the density of amorphous linear PAAm (ρ = 1.445 × 10^3 kg/m^3) was employed as ρ_N needed for the evaluation of $\Delta\rho$. The density of the linear PAAm with M_w = 1.0 × 10^4

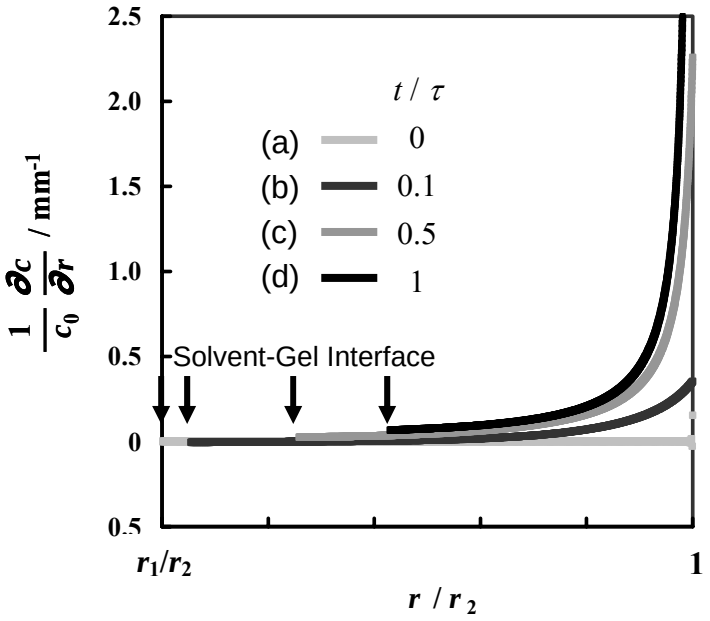

Figure 4-5 A normalized concentration gradient, $(\partial c / \partial r)/c_0$ inside gel as a function of r/r_2. (a) for $t / \tau = 0$, (b) for $t / \tau = 0.1$, (c) for $t / \tau = 0.5$, (d) for $t / \tau = 1$.

g/mol was evaluated from the densities of the aqueous solutions with various PAAm concentrations assuming the additivity for volume.

4.3.2 Measurements

Measurements were made using an analytical ultracentrifuge (Beckman, Spinco Model E) with a light of Hg e-line (546 nm) at 25 ^{o}C. A single-sector 12-mm cell with quartz glass window was employed. The centerpiece of the cell is made of poly(trifluorochloroethylene) to minimize the friction between the cell wall and the gel. The initial dimension of the gel in centrifugal direction is about 9 mm, and the thickness and width, both of them are unchanged under centrifugal fields, are 12 and 4 mm, respectively. The measurements were carried out at the rotor speed of 1.80×10^4 or 6.00×10^4 rpm. The Schlieren diagrams photographed were read on a contour projector (Nippon Kogaku, L-16) to the accuracy of ±0.001mm.

4.4 Results and Discussion

Figure 4-6 displays the Schlieren patterns during the shrinking of the PAAm gel at the centrifugal acceleration of $\alpha = 2.26 \times 10^4$ G. In these patterns, each position of air-solvent and solvent-gel interfaces is evidently recognizable as the point where the concentration gradient diverges. At $t = 6.00 \times 10^2$ s, the air-solvent and solvent-gel interfaces are not distinguishable because the rotation time is too short to yield a finite shrinking. At $t = 9.38 \times 10^4$ s (ca. 1 day), an appreciable shift of the solvent-gel interface toward the cell bottom (i.e., shrinking) is visible, while the air-solvent interface is immobile due to the incompressibility of the solvent. After sufficiently long time to achieve the stationary state ($t = 6.95 \times 10^5$ s), the length of the gel decreases to less than a

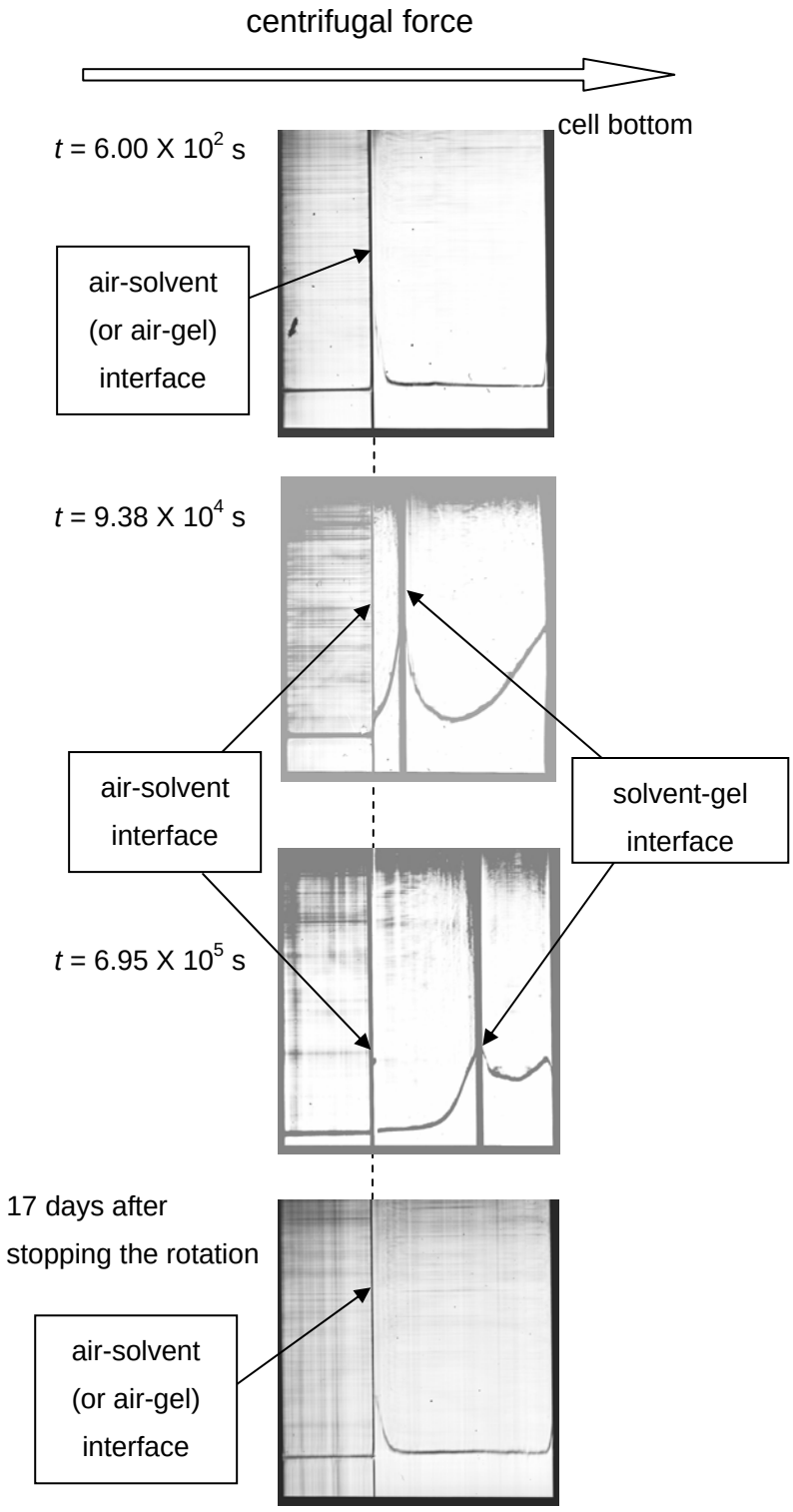

Figure 4-6 The Schlieren patterns in the shrinking process of a PAAm gel at the centrifugal acceleration $\alpha = 2.26 \times 10^4$ G as a function of time. The last column shows an example of the patterns sufficiently long after stopping the rotation.

half of the initial length. It should be noticed in the last column in Figure 4-6 that the position of the solvent-gel interface shifted by the centrifugal force slowly returns to the original position after stopping the rotation. This indicates that the deformation induced by centrifugal forces is recoverable; that no irreversible structural change in the gel is caused by the centrifugal forces. Near the bottom of the cell, the concentration gradient increases with time. This upturn of the concentration gradient is qualitatively corresponding with the calculation results of Equation (4.14) (Figure 4-5). It is, however, difficult to completely reproduce the change of the concentration gradient by the theory because the unreacted monomers are included inside the gel. The time course of the change in the concentration gradient may reflect the sedimentation process of the unreacted monomers, but it is beyond the scope of the present study to enter into the details.

Figure 4-7 illustrates the position of the moving surface of the gels (i.e., the gel-solvent interface) as a function of time at $\alpha = r_i\Omega^2/g = 2.26 \times 10^4$ or 2.57×10^5 G. The value of r at $t = 0$ (r_i) corresponds to the initial distance of the gel surface from the rotation center before applying the centrifugal force. In the case of $\alpha = 2.26 \times 10^4$ G, the shrinking proceeds linearly with time in the short time region, while the steady state of shrinking is achieved in the long time region (after ca. 6 days). The extrapolation from the data in the short time region to $t = 0$ slightly deviates from the data at $t = 0$, resulting from the fact that a finite time (ca. 7 min) is required to reach the constant rotation speed in the experiments. Thus we employ the intercept at $t = 0$ in the linear extrapolation as r_i for further analysis. At the higher centrifugal acceleration of $\alpha = 2.57 \times 10^5$ G, the shrinkage also increases linearly with time, and the shrinking rate is about 1

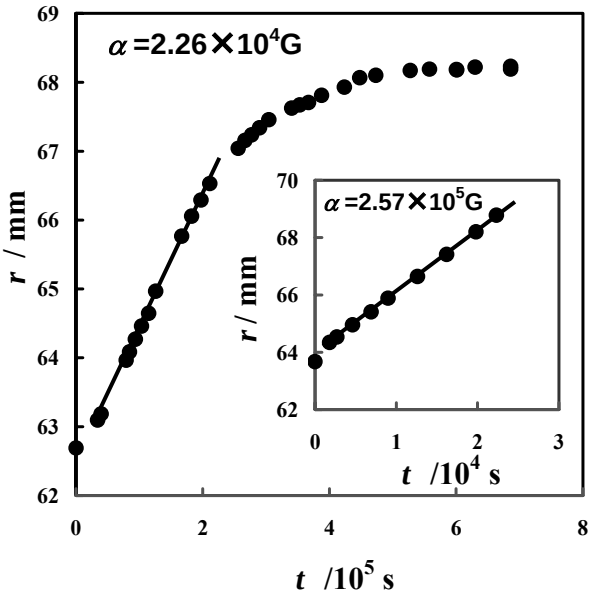

Figure 4-7 Position of the solvent-gel interface (the moving surface) of a PAAm gel as a function of time at the centrifugal acceleration of $\alpha = 2.26 \times 10^4$ G. The inset shows the same plots for the data at $\alpha = 2.57 \times 10^5$ G. The straight lines represent the linear regression in the short time region. The deviations of the data at t=0 from the linear extrapolations result from the fact that a finite time (ca. 7 min) is required to achieve each constant rotation speed.

order of magnitude larger than that at $\alpha = 2.26 \times 10^4$ G. Meanwhile, the true value of stationary shrinking is not attainable at $\alpha = 2.58 \times 10^5$ G, because the high centrifugal force yields such a large shrinking that the shift of the gel surface stops due to the presence of the bottom wall (located at $r = 71.76$ mm).

According to Equations (4.10) and (4.11), the modulus L and the friction coefficient f can be evaluated from the stationary shrinkage and the initial shrinking rate, respectively. For the calculations, $r_1 = 6.240 \times 10^{-2}$ m and $r_2 = 7.174 \times 10^{-2}$ m for $\alpha = 2.26 \times 10^4$ G; $r_1 = 6.395 \times 10^{-2}$ m and $r_2 = 7.176 \times 10^{-2}$ m for $\alpha = 2.57 \times 10^5$ G were used together with $\phi = 2.09 \times 10^{-2}$ and $\Delta\rho = \rho_N - \rho_{water} = 4.48 \times 10^2$ kg/m^3. From Equation (4.11) and the linear regression for the data in the short time region at $\alpha = 2.26 \times 10^4$ and 2.58×10^5 G, f is estimated to be 1.04×10^{14} and 1.10×10^{14} Ns/m^4, respectively. The data at different α yield almost the same value of f, indicating that the initial shrinking rate is proportional to α as expected from the theory. These f values are also close to $f = 1.5 \times 10^{14}$ Ns/m^4 obtained by a frictional measurement[8] of the PAAm gel with the same concentrations of monomer and cross-linker as the PAAm gel in the present study. From Equation (4.11) with $r_\infty = 6.820 \times 10^{-2}$ m at $\alpha = 2.26 \times 10^4$ G, L is evaluated to be 1.64×10^4 Pa. These values of f and L yield $D = 1.57 \times 10^{-10}$ m^2/s.

Figure 4-8 displays the result of the curve fit based on Equation (4.12) to the whole time dependence of the data at $\alpha = 2.26 \times 10^4$ G. In the fitting, τ_L and L were used as adjustable parameters while other parameter values were the same as aforementioned values. The theoretical curve satisfactorily fits the data, although each of the initial shrinking rate and stationary shrinkage in the fitted curve is slightly larger than that in the data. The fitted values of τ_L and L are

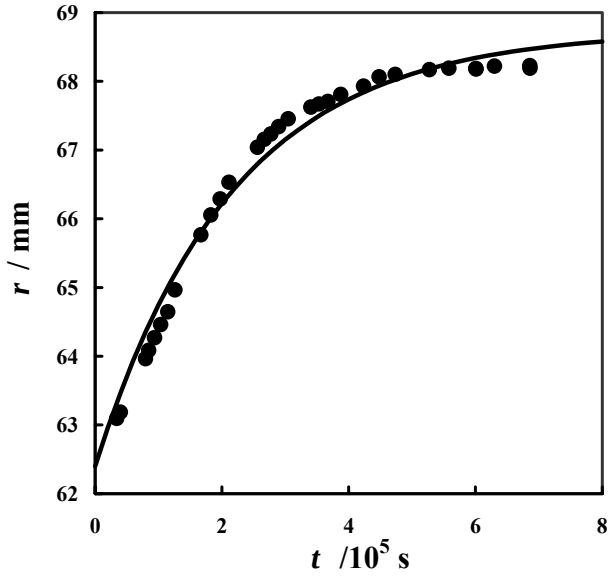

Figure 4-8 The comparison of the experimental data at $\alpha = 2.26 \times 10^4$ G with the best-fitted curve of Equation (4.12). The fitted values of τ_L and L are 2.16×10^5 s and 1.50×10^4 Pa, respectively.

2.16×10^5 s and 1.50×10^4 Pa, respectively. These yield $f = 9.17 \times 10^{13}$ Ns/m^4 and $D = 1.64 \times 10^{-10}$ m^2/s. Each value of L, f and D obtained in the curve fitting well accords with that evaluated from the stationary shrinkage and initial shrinking rate as mentioned above, respectively.

Thus the experimental data on the shrinking of the PAAm gel under ultracentrifugal fields are well explained by the theory proposed in this chapter. Further, the present work has demonstrated that the ultracentrifugal measurements of gels enable us to evaluate simultaneously f and L of polymer networks.

4.5 Conclusions

Ultracentrifugal fields induces the shrinking of gels. In the short time region, the shrinking proceeds at a constant rate, while the shrinking reaches the stationary state in the long time limit. A theory is proposed to describe the diffusion process of networks in the presence of centrifugal fields. The theory demonstrates that the initial shrinking rate is dominated by the ratio of the frictional force and the centrifugal force; that the stationary shrinkage is determined by the balance between the elastic force and the centrifugal force; that the whole shrinking process substantially obeys a single exponential relaxation whose characteristic time is proportional to the ratio of the square of the stationary displacement and the diffusion constant of networks. The whole shrinking process of a polyacrylamide gel under ultracentrifugal fields observed is satisfactorily described by the theory. The analysis based on the theory enables us to evaluate the friction constant as well as the longitudinal elastic modulus of the network.

References

1. T. Tanaka, L. O. Hocker, and G. B. Benedek, *J. Chem. Phys.*, **59**, 5151 (1973)
2. T. Tanaka, and D. J. Fillmore, *J. Chem. Phys.*, **70**, 1214 (1979)
3. A. Peters, and S. J. Candau, *Macromolecules*, **21**, 2278 (1988)
4. Y. Li, and T. Tanaka, *J. Chem. Phys.*, **92**, 1365 (1990)
5. A. Onuki, in "*Responsive Gels: Volume Transition I*", K. Dusek ed., *Adv. Polym. Sci.*, (Springer-Verlag, Berlin and Heidelberg, 1993), Vol. 109, 63
6. C. Wang, Y. Li, and Z. Hu, *Macromolecules*, **30**, 4727 (1997)
7. T. Yamaue, and M. Doi, *Phys. Rev. E*, **69**, 041402 (2004)
8. M. Tokita, and T. Tanaka, *J. Chem. Phys.*, **95**, 4613 (1991)
9. T. Takigawa, K. Uchida, K. Takahashi, and T. Masuda, *J. Chem. Phys.*, **111**, 2295 (1999)
10. T. Takigawa, K. Urayama, Y. Morino, and T. Masuda, *Polymer Journal*, **25**, 929 (1993)
11. T. Takigawa, K. Urayama, and T. Masuda, Polym. *Gels and Networks*, **2**, 59 (1994)
12. K. Urayama, T. Takigawa, and T. Masuda, *Rheol. Acta*, **33**, 89 (1994)
13. A. Suzuki, and H. Hara, *J. Chem. Phys.*, **114**, 5012 (2001)
14. S. Sasaki, *J. Chem. Phys.*, **120**, 5789 (2004)
15. S. Hirotsu, *Macromolecules*, **37**, 3415 (2004)
16. L. D. Landau, and E. M. Lifshitz, "*Theory of Elasticity*", Pergamon Press, Oxford, 1986

Chapter 5

Kinetics of Shrinking of Poly(vinyl alcohol) Gels Induced by Ultracentrifugal Fields

5.1 Introduction

In Chapter 4, the shrinking behavior of the polyacrylamide gels under ultracentrifugal forces are investigated, and we successfully estimated the frictional coefficient between solvent and the networks on the basis of the model that we proposed. It is known that the frictional property of the polymer network contributes to solvent permeability though the gels. Control of the permeation of low molecular weight substances through a membrane is a key to the separation technique. Permeability as well as selectivity is strongly affected by the structure of membranes. To utilize a polymer gel as a membrane, studies on the frictional properties of the gel membranes becomes very important. However, there exist only a few studies[1-4] on the frictional or solvent flow properties of the polymer gels. A limited number of the studies on the friction is mainly due to the difficulty of experiment; of course, no commercial apparatus is available for the measurements. Thus, it is meaningful that the measuring methods of the frictional properties of polymer gels are established. We have shown in Chapter 4 that a ultracentrifuge is available to estimate the frictional coefficient of the "chemical" gels, i.e., polyacrylamide gels whose cross-links are formed by covalent bonds. To establish the new measuring method by using the ultracentrifuge, the frictional properties of various types of polymer gels must be

measured with the same method. In this chapter, we treat the Poly(vinyl alcohol) gals cross-linked by microcrystallites which are classified into “physical gels” The shrinking behavior of the physical gels under ultracentrifugal forces have not been investigated before. The frictional coefficient of PVA gels is estimated by an untracentifuge, and the data are analyzed in terms of the theory proposed in Chapter 4. In addition, the centrifugal acceleration dependence of shrinking kinetics of the gels which is not examined for the PAAm gels in Chapter 4, is investigated.

5.2 Experimental

5.2.1 Materials

Poly(vinyl alcohol) (PVA) with the degree of polymerization of 1700 and the degree of saponification of 99.5 mol% was kindly supplied from Unitika, Japan. PVA was dissolved in a mixed solvent of water and dimethyl sulfoxide (DMSO) at 80 °C for 1 h. The ratio of water to DMSO was 1:4 by weight. Polymer concentration was fixed to be 3.2 wt%. After the complete dissolution of PVA, the solution was transferred to the cell of the ultracentrifuge and was gelled inside the cell at -20 °C for 24 h.

In analyzing the experimental data, the following values and methods were used. The density of PVA ρ_{pva} is 1.269×10^3 kgm^{-3}.[5] The density of the mixed solvent ρ_{sol} was measured at 25 °C to give $\rho_{sol} = 1.0943 \times 10^3$ kgm^{-3}. The volume fraction of the polymer network ϕ was calculated by assuming additivity of volume for the polymer and the mixed solvent, leading to $\phi = 0.028$. From another experiment the fraction of the soluble PVA, not incorporated into the

infinite network after gelation, in the system (the sol-fraction) was estimated to be 17 wt%. The relating high sol-fraction originates from the fact that the PVA concentration (3.2 wt%) is very close to the critical concentration for gelation. The gel with high concentration showed no finite displacement under the ultracentrifugal force owing to the large elastic modulus.

5.2.2 Measurements

The shrinking behavior of the PVA gels were observed by the same ultracentrifuge shown in Chapter 4. The operations were carried out at various rotational speeds (3.00×10^4, 4.00×10^4, 4.80×10^4, 5.20×10^4, 5.60×10^4, and 6.00×10^4 rpm) at 25 °C. The cell used in this study was the same one as used in Chapter 4 so that the cross-sectional area of the samples is same. The length of the gels in the moving direction ranges from 8 to 9 mm.

5.3 Results and Discussion

Figure 5-1 shows the Schlieren patterns of the PVA gel at the centrifugal acceleration α (= $r_1\Omega^2 / g$) of 2.53×10^5 G (6.00×10^4 rpm) where g represents the gravitational acceleration. At the shortest time (t = 8.40×10^2 s) only one vertical line is observed (Figure 5.1a). This corresponds to the overlapped line of the air-solvent and solvent-gel interfaces. On the patterns at $t > 8.4 \times 10^2$ s (Figures. 5.1b ~ 5.1d) each of the air-solvent and the solvent-gel interfaces is clearly emerged as a divergence. The patterns inside the gel show no peak except for the region near the bottom, while a peak is observed on the patterns in the solvent region lying between the two divergent lines. The upturn near the

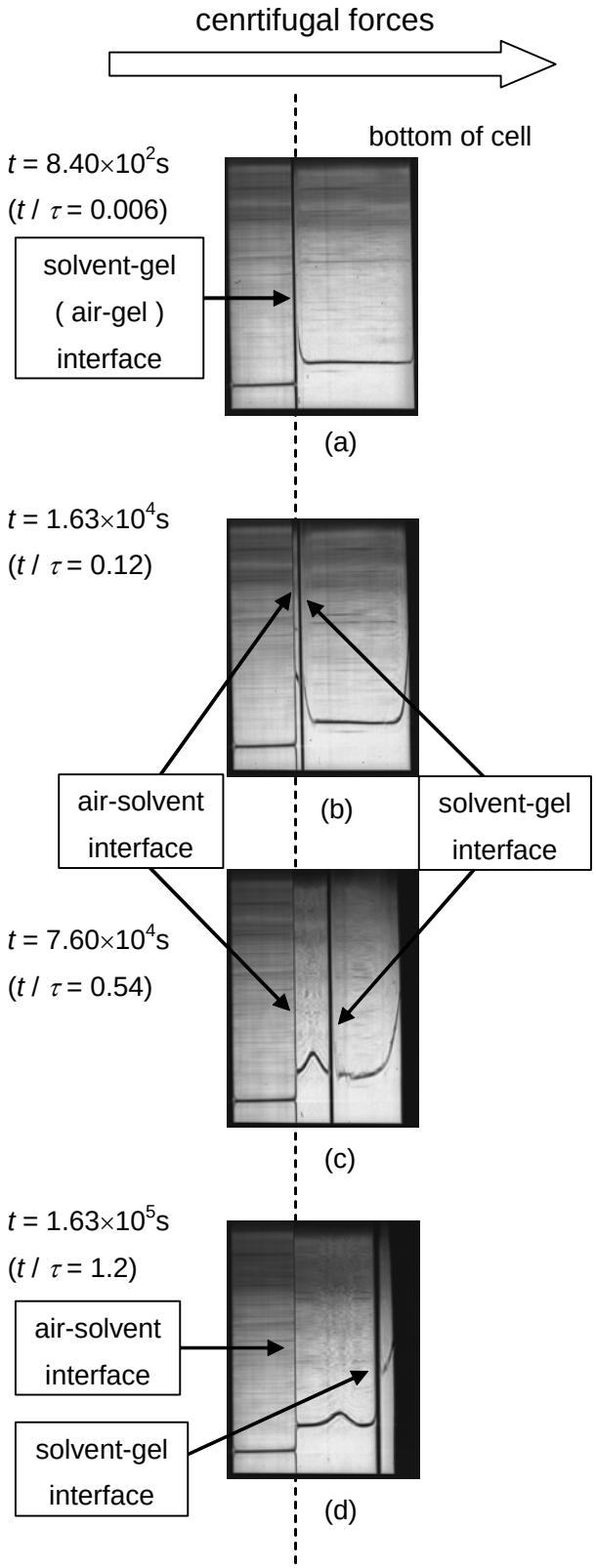

Figure 5-1 Schlieren patterns in the course of centrifugation at the angular velocity (Ω) of 5.73 x 10^5 s^{-1}. (a) at t = 8.40 × 10^2 s; (b) at t = 1.63 × 10^4 s; (c) at t = 7.60 × 10^4 s; (d) at t = 1.63 × 10^5 s.

bottom originates from the high condensation of the polymer network and the peak in the solvent region is due to the sedimentation of free PVA chains existing the solvent phase. The sedimentation of the free chains and infinite networks obey different equations of motion, although their densities are comparable. The analysis of the sedimentation of free chains excluded from the gel is beyond the scope of this study. At $t = 1.63 \times 10^4$ s the solvent-gel interface moves slightly and becomes distinguished from the air-solvent interface. At $t = 7.60 \times 10^4$ s the solvent-gel interface moves further toward the bottom of the cell while the air-solvent interface remains at the initial position. The peak near the bottom appears to be larger, and the character is qualitatively reproduced on the calculated curves shown in Chapter 4 (Figure 4-5). At long times (for example, $t = 1.63 \times 10^5$ s), the solvent-gel interface becomes close to the bottom. The moving interface reaches the stationary state.

Figure 5-2 shows the time dependence of the position of the solvent-gel interface for the same PVA gel in Figure 5-1. At short times ($t < 7.8 \times 10^3$ s), the displacement appears to be a little small probably because the rotation speed did not reach the steady rotation speed. In the middle region of t (7.8×10^3 s $< t < 1.3 \times 10^5$ s), the interface moves toward the bottom of the cell and the change in position is in proportion to time. In the late stage, the displacement becomes small with increasing time and finally the position of interface levels off to show a constant value ($r \cong 70$ mm). The position at the cell bottom corresponds to r of 71.73 mm. This is very close to the saturated value of r (ca. 70 mm) observed from the experiment, suggesting that the gel sample becomes rather dense due to a stronger centrifugal force. From a simple calculation we found that the volume of the gel at $t = 2.8 \times 10^5$ s (longest time measured) corresponds to about 1/10 of

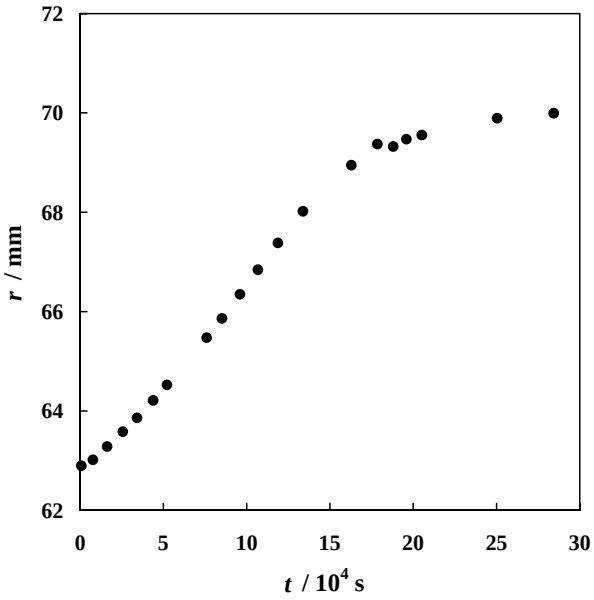

Figure 5-2　Time (t) dependence of the position at the solvent-gel interface (r) for a PVA gel at the angular velocity (Ω) of 5.73×10^5 s^{-1}.

the initial volume; still, the polymer concentration remains around 32 wt% since the concentration becomes 10 times higher than the initial one (3.2 wt%). The sample can be regarded as a polymer gel even in the collapsed state, ensuring that the estimation of the characteristic time is meaningful. The longest characteristic time in the course of compression (τ) was obtained as 1.4×10^4 s.

As shown in Chapter 4, the motion of the solvent-gel interface can be described in terms of $u(r_1, t)$. In the initial stage of the centrifugation ($t \ll \tau_L$), $u(r_1, t)$ is approximated by a linear term of t and is written as

$$u(r_1, t) \cong \frac{\phi \Delta \rho r_1 \Omega^2}{f} t \tag{5.1a}$$

If the shrinking velocity v is used,

$$v(r_1, t) \equiv \frac{d}{dt} u(r_1, t) \cong \frac{\phi \Delta \rho r_1 \Omega^2}{f} \tag{5.2b}$$

The plots of r vs. t for the PVA gels are shown in Figure 5-3. The figure contains several groups of data differing in Ω, but other parameters are almost the same for all runs (or samples). In the region of t shown in the figure, each set of the data falls on a line. The slope of the line appear to increase with increasing Ω. As stated previously, the slope is theoretically given by Equation (4.11): The slope becomes equal to $\phi \Delta \rho r_1 \Omega^2 / f$. Figure 5-4 shows the double-logarithmic plots of v against Ω for the PVA gels. The line in the figure has the slope of 2 and the data points appear to be well represented by the line, suggesting that the relation $v \propto \Omega^2$ expected by the theory holds. In Figure 5-5 v is plotted against α. The velocity v is proportional to α. This linear relation allows us to estimate an average value of f from the slope of the line, $\phi \Delta \rho g / f$. The value lies about 3.5×10^{14} Nsm^{-4}. This value of the friction coefficient was almost the same value reported in previous study of the PVA gels where the

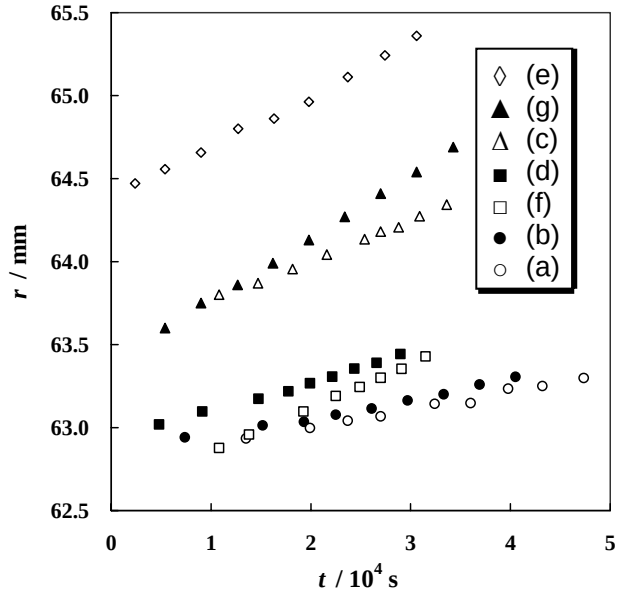

Figure 5-3 Time (t) dependence of the position at the solvent-gel interface (r) for a PVA gel at the various angular velocities (Ω). (a) 2.86×10^5 s^{-1}, (b) 3.82×10^5 s^{-1}, (c) 4.58×10^5 s^{-1}, (d) 4.97×10^5 s^{-1}, (e) 5.35×10^5 s^{-1}, (f) 5.35×10^5 s^{-1} , (g) 5.73×10^5 s^{-1}.

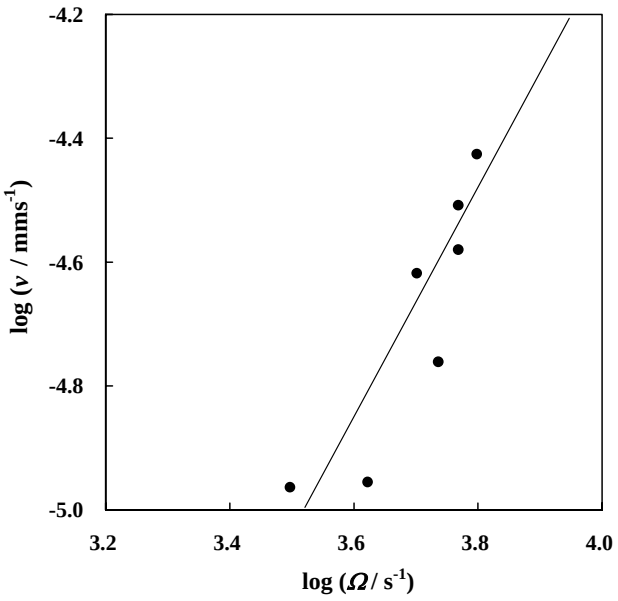

Figure 5-4 Double-logarithmic plots of the velocity (v) against angular velocity (Ω) for PVA gels. The line in the figure has the slope of 2.

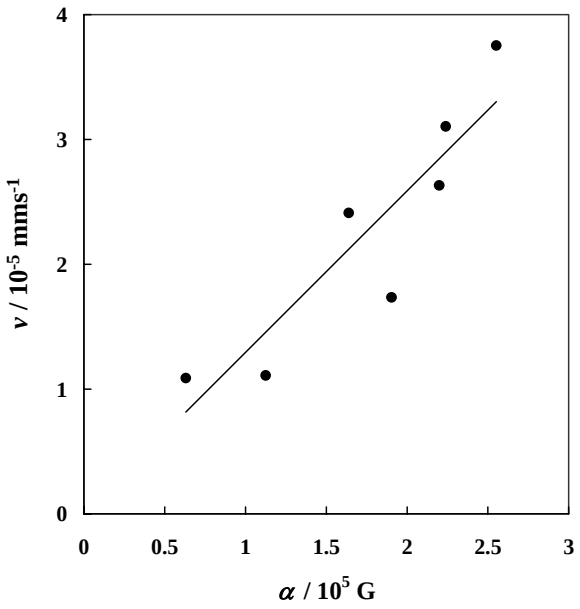

Figure 5-5 Plots of the velocity (v) against centrifugal acceleration (α) for PVA gels. The line in the figure is determined by the method of least-squares.

conditions of the measurement were somewhat different from this study.[3]

5.4 Conclusions

The compressive behavior of the PVA gels under ultracentrifugal forces was investigated and the profiles of the concentration gradient of the gels obtained by experiment were compared with the theoretical prediction. When the centrifugal force is applied to the gel, the concentration gradient near the bottom of the cell increases sharply whereas the gradient remains almost constant in the region far from the bottom. Further application of the centrifugal forces enhances the peak near the bottom. These are well explained by the theory. The Ω-dependence of the position at the solvent-gel interface measured shows that the velocity of the interface is proportional to Ω^2, as is predicted by the theory. The frictional coefficient f of the PVA gels is estimated to be 3.5×10^{14} Nsm^{-4}.

References

1. M. Tokita, and T. Tanaka, *J. Chem. Phys.*, **95**, 613 (1991)
2. T. Tanaka, S. Ishiwata, and C. Ishimoto, *Phys. Rev. Lett.*, **38**, 771 (1977)
3. T. Takigawa, K. Uchida, K. Takahashi, and T. Masuda, *J. Chem. Phys.*, **111**, 2295 (1999)
4. T. Takigawa, K. Uchida, K. Takahashi, and T. Masuda, *Biorheology*, **36**, 401 (1999)
5. I. Sakurada, Y. Nukushina, and Y. Sone, *Kobunshi Kagaku*, **12**, 506 (1955)

Chapter 6

Steady Flow Properties of Mixed Solvent through Poly(*N*-isopropylacrylamide) Gels

6.1 Introduction

As stated in Chapter 1, the degree of swelling of the polymer gels have been experimentally and theoretically investigated. The degree of swelling (Θ) is one of the important parameters of the gels, because Θ affects their moduli.[1-3] Generally, Θ of polymer gels is governed by various parameters such as solvent quality and temperature.[4-10] When a mixed solvent is used as a swelling solvent, Θ is expected to depend on the solvent composition. Swelling behavior of the gels in mixed solvents have been examined both by theory and experiment.[4,5,9-12] In the studies employing mixed solvents, the swelling characteristics of polymer gels are described in terms of the solvent composition of the surrounding solvent because the composition is easy to control and thus becomes a good variable. However, the composition of the solvent inside gels has been undetermined although the importance of the determination is widely understood. This is chiefly because there are few methods conveniently applicable to the detection. In this chapter, we propose the determination method of the solvent composition inside the polymer gels.

In Chapters 4 and 5, the frictional coefficient between solvent and the polymer network f is mentioned, and it is well known that f governs the solvent flow through the gel. In the previous study,[13] the flow properties of a solvent

through poly(vinyl alcohol) hydrogels membranes were investigated, and the results indicates that the flow rate is closely related to the increase of Θ. Although some studies concerning the permeation properties of solvents through gels have been reported,[14-17] few studies on the permeation properties of mixed solvents through highly swollen polymer gel membranes have been reported. In this chapter, we employ a combination of a poly(*N*-isopropylacrylamide) (PNIPA) gel and water (W) / *N*,*N*-dimethylformamide (DMF) binary mixture and investigate the frictional properties. Among the good solvents for PNIPA we chose these solvents because they are almost the same in density but have a large difference in the refractive index through which the solvent composition is determinable. The dependence of Θ on the solvent composition is also examined for the PNIPA gels. In the next section, a simple model to describe the swelling and solvent flow properties of polymer gels is presented. The solvent composition inside the gels is estimated on the basis of the model.

6.2 Model

Consider a flow of a mixed solvent through an isotropic and highly swollen polymer gel membrane. As shown in Figure 6-1, the situation is that an upstream side of the gel membrane is in contact with a binary solvent, a mixture of the miscible solvent 1 and solvent 2, under a hydrostatic pressure (p) and the penetrant from the downstream side is immediately restored. The membrane is assumed to be freely swellable; hence, the swelling ratio of the membrane depends on p as well as the solvent composition. The usual definition of the separation coefficient (α) has been made by using the molar concentration, but

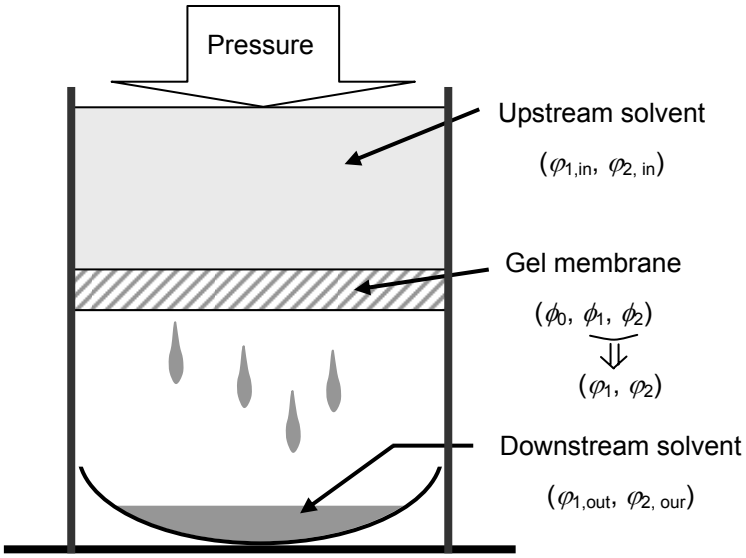

Figure 6-1 The schematic representation of the permeation through the gel membrane for the binary solvent system.

in this chapter α is defined in terms of the volume fraction as

$$\alpha = \left(\frac{\varphi_{1,\mathrm{out}}}{\varphi_{2,\mathrm{out}}} \right) \Big/ \left(\frac{\varphi_{1,\mathrm{in}}}{\varphi_{2,\mathrm{in}}} \right) \tag{6.1}$$

where $\varphi_{1,\mathrm{in}}$ and $\varphi_{1,\mathrm{out}}$ are the volume fraction of the solvent i (i=1, 2) in the upstream and the downstream solvent phases, respectively. Of course, we have the relations that $\varphi_{1,\mathrm{in}} + \varphi_{2,\mathrm{in}} = 1$ and $\varphi_{1,\mathrm{out}} + \varphi_{2,\mathrm{out}} = 1$.

6.2.1 Solvent Composition inside Gel Membranes in the Steady State

When the steady flow is achieved, the (equilibrium) thermodynamics must be applied to the solvent partition between the solvent and gel phases at the upstream interface. In case that p is not so high, the effects of p on the thermodynamic quantities can be neglected. A simple calculation under these assumptions leads to the equilibrium swelling ratio of the gel membrane and the solvent composition inside the gel. Let ϕ_0, ϕ_1 and ϕ_2 be the volume fractions of the polymer network, solvent 1 and solvent 2, respectively. These fractions are related to one another by

$$\phi_0 + \phi_1 + \phi_2 = 1 \tag{6.2}$$

and then the degree of swelling Θ is given by $\Theta = 1 / \phi_0$. The mixing free energy (ΔG) based on a lattice model is given by[18]

$$\frac{\Delta G}{kT} = N_1 \ln\phi_1 + N_2 \ln\phi_2 + (N_0 + N_1 + N_2)(\chi_{01}\phi_0\phi_1 + \chi_{02}\phi_0\phi_2 + \chi_{12}\phi_1\phi_2) + \frac{3}{2}\nu\phi_0^{-3/2} \tag{6.3}$$

where k is the Boltzmann constant and T is the temperature, N_i (i = 1, 2) being the number of molecules of the solvent i. The quantity N_0 is the total number of polymer segments and ν is the number of active chains in the network, so that N_0/ν ($\equiv n$) gives the average number of polymer segments between crosslinks.

The quantity χ_{0i} (i=1, 2) is the interaction parameter between the network and solvent i, and χ_{12} is the interaction parameter between solvents 1 and 2. The chemical potential change by mixing for the solvents 1 and 2 ($\Delta\mu_1$ and $\Delta\mu_2$, respectively) are written by

$$\frac{\Delta\mu_1}{kT} = \ln\phi_1 + 1 - \phi_1 - \phi_2 + \chi_{01}\phi_0(\phi_0 + \phi_2) - \chi_{02}\phi_0\phi_2 + \chi_{12}\phi_2(\phi_0 + \phi_2) + \frac{1}{n}\phi_0^{1/3} \tag{6.4a}$$

$$\frac{\Delta\mu_2}{kT} = \ln\phi_2 + 1 - \phi_1 - \phi_2 - \chi_{01}\phi_0\phi_1 + \chi_{02}\phi_0(\phi_0 + \phi_1) + \chi_{12}\phi_1(\phi_0 + \phi_1) + \frac{1}{n}\phi_0^{1/3} \tag{6.4b}$$

At equilibrium in contact with the outside solvent, the chemical potentials must satisfy the conditions: $\Delta\mu_1/kT = \ln\varphi_{1,\text{in}} + \chi_{12}\varphi_{2,\text{in}}^2$ and $\Delta\mu_2/kT = \ln\varphi_{2,\text{in}} + \chi_{12}\varphi_{1,\text{in}}^2$. Accordingly, we have the following equations as equilibrium conditions:

$$\ln\phi_1 + 1 - \phi_1 - \phi_2 + \chi_{01}\phi_0(\phi_0 + \phi_2) - \chi_{02}\phi_0\phi_2 + \chi_{12}\phi_2(\phi_0 + \phi_2) + \frac{1}{n}\phi_0^{1/3} = \ln\varphi_{1,\text{in}} + \chi_{12}\varphi_{2,\text{in}}^2 \tag{6.5a}$$

$$\ln\phi_2 + 1 - \phi_1 - \phi_2 - \chi_{01}\phi_0\phi_1 + \chi_{02}\phi_0(\phi_0 + \phi_1) + \chi_{12}\phi_1(\phi_0 + \phi_1) + \frac{1}{n}\phi_0^{1/3} = \ln\varphi_{2,\text{in}} + \chi_{12}\varphi_{1,\text{in}}^2 \tag{6.5b}$$

Equations (6.2) and (6.5) determine the volume fractions of the polymer and solvents inside the membrane in the steady state. For simplicity, we write a set of solutions formally as (ϕ_0, ϕ_1, ϕ_2). For the further calculation, however, it is more convenient to transform the solution set in another form:

$$\phi_0 = \phi \tag{6.6a}$$

$$\phi_1 = (1 - \phi)\varphi_1 \tag{6.6b}$$

$$\phi_2 = (1 - \phi)\varphi_2 \tag{6.6c}$$

where φ_i (i = 1, 2) is the volume fraction of the solvent i in the mixed solvent; hence, $\varphi_1+\varphi_2$=1. The variables ϕ, φ_1 and φ_2 are functions of $\varphi_{1,\text{in}}$ and $\varphi_{2,\text{in}}$. The network fraction ϕ in the gel membrane can be written by Equation (6.5) as

$$\phi = -\frac{1}{(\chi_{01}-\chi_{02})-\chi_{12}(\varphi_2-\varphi_1)}\left[\chi_{12}\left(\varphi_{2,\mathrm{in}}^2-\varphi_{1,\mathrm{in}}^2\right)-\chi_{12}(\varphi_2-\varphi_1)-\ln\frac{K_1}{K_2}\right] \tag{6.7}$$

where, K_i (i=1, 2) defined by the equation below corresponds to the partition coefficient for the solvent i.

$$K_\mathrm{i} = \frac{\varphi_\mathrm{i}}{\varphi_{\mathrm{i,in}}} \tag{6.8}$$

6.2.2 Solvent Flow inside the Membrane

In this section, we consider a one-dimensional flow of the binary solvent inside a highly swollen ($\phi << 1$) polymer gel. Let the positions of upstream and downstream interfaces be x=0 and x=d, respectively. According to the two-fluid model, the volume-averaged solvent velocity v at position x ($0 \le x \le d$) and time t is given by

$$v(x,t) = \varphi_1(x,t)v_1(x,t) + \varphi_2(x,t)v_2(x,t) \tag{6.9}$$

where $\varphi_\mathrm{i}(x, t)$ and $v_\mathrm{i}(x, t)$ (i=1, 2) are the local volume fraction and the local solvent velocity of the species i, respectively. Darcy's law for each solvent flow can be written by

$$-f_\mathrm{i}\varphi_\mathrm{i}(x,t)v_\mathrm{i}(x,t) = \frac{\partial}{\partial x}\left[\varphi_\mathrm{i}(x,t)p(x,t)\right] \tag{6.10}$$

with f_i (i=1, 2) being the frictional coefficient for the solvent i and the $p(x, t)$ being the applied pressure. Because the gel membrane is swellable, the solvent mass conservation leads to the following relations.

$$-\frac{\partial}{\partial t}\varepsilon_\mathrm{i}(x,t) = \frac{\partial}{\partial x}\left[\varphi_\mathrm{i}(x,t)v_\mathrm{i}(x,t)\right] \tag{6.11}$$

In the above equation, ε_i is the elongational strain originating from the swelling by the solvent i and the total strain ε is given by $\varepsilon(x, t)=\varepsilon_1(x, t)+\varepsilon_2(x, t)$. It is

noted that the elongational strains directly correspond to the volume changes because the flow we consider here is one-dimensional. The strains, ε_i (i= 1, 2) is related to the applied pressure $p(x, t)$ and the volume fraction as

$$\varepsilon_i(x,t) = \frac{\varphi_i(x,t)p(x,t)}{K_{OS} + (4/3)G} \tag{6.12}$$

This corresponds to the linear constitutive equation for the gel membrane. The constants K_{os} and G are the osmotic bulk modulus and the shear modulus, respectively. From Equations (6.10)-(6.12) we have diffusion-type equation for i =1, 2.

$$\frac{\partial}{\partial t}[\varphi_i(x,t)p(x,t)] = D_i \frac{\partial^2}{\partial x^2}[\varphi_i(x,t)p(x,t)] \tag{6.13}$$

and the constant D_i is given by

$$D_i = \frac{K_{os} + (4/3)G}{f_i} \tag{6.14}$$

The steady solutions for a set of Equation (6.13) under the boundary conditions, $p(x=0)=p_0$, $p(x=d)=0$ and $\varphi_1(x=0)=\varphi_1$, are given as follows.

$$p(x) = p_0\left(1 - \frac{x}{d}\right) \tag{6.15a}$$

$$\varphi_1(x) = \varphi_1 = const \tag{6.15b}$$

$$\varphi_2(x) = 1 - \varphi_1 = const \tag{6.15c}$$

These leads to the steady flow rate (Q_i) (i=1, 2) per unit interface area at $x=d$ as

$$Q_i(d) \equiv -\frac{1}{f_i}\left[\frac{\mathrm{d}}{\mathrm{d}x}\{\varphi_i(x)p(x)\}\right]_{x=d} = \frac{\varphi_i p_0}{f_i d} \tag{6.16}$$

The reciprocal of f_i can also be called the permeability for the solvent i. The ratio $\varphi_{1,out}/\varphi_{2,out}$ becomes identical to $Q_1(d)/Q_2(d)$. Generally, the separation coefficient α cannot be expressed by a simple form. However, if χ_{12} = 0 then we have from Equations (6.1) and (6.7)

$$\alpha = \frac{f_2}{f_1} \exp[-(\chi_{01} - \chi_{02})\phi] \tag{6.17}$$

6.3 Experimental

6.3.1 Materials

Poly(*N*-isopropylacrylamide) (PNIPA) hydorogel membranes were prepared by radical copolymerization of NIPA and BIS by the same way as Chapters 2 and 3. The total monomer concentration of NIPA and BIS was fixed to 10wt%, the molar ratio [NIPA] / [BIS], a measure of the crosslink density, was settled to be 100. The pregel solutions were cast on a glass plate, and the gelation was performed between sandwiched glass plates with a spacer for 24 hours at 5 °C. The concentrations of AP and TEMED were 0.8 g/l and 2.4 ml/l, respectively. The gel membranes were removed from the glass plates and were poured into distilled water to eliminate unreacted reagents. The surrounding water was exchanged for several times until the gel membranes reach to swelling equilibrium. The thickness of the gel membranes in equilibrium was ca. 500 μm. For swelling experiments, cylindrical gels were prepared by using the same pregel solutions. The gelation was performed in a glass capillary with an inner diameter of 3.32 mm. The obtained cylindrical gels were immersed into distilled water to wash out the unreacted regents.

6.3.2 Swelling Measurements

The swelling experiments were made at atmospheric pressure. The degree of swelling of the PNIPA gels (Θ) at 20 °C was calculated by the ratio of volume of the swollen gel (V) to that of the dried gel (the polymer network)

(V_{dry}). The volume of dried gel was calculated by the volume (V_{gel}) and weight (W_{gel}) of a swollen gel by water and the weight of the dried gel (W_{dry}) by assuming the additivity between water and PNIPA. The value of V_{dry} can be written as

$$V_{dry} = V_{gel} - V_{water} = V_{gel} - \frac{W_{gel} - W_{dry}}{\rho_{water}} \tag{6.18}$$

where V_{water} and ρ_{water} stand for the volume of water inside the gel and the density of water, respectively. The specific gravity of the polymer network (W_{dry}/V_{dry}) was determined to be 1.15 at 20 ^{o}C. Since Θ for the gels in the mixed solvent can be written by using the volume in water V_w as

$$\Theta = \frac{V}{V_{dry}} = \frac{V_W}{V_{dry}} \frac{V}{V_W} = \frac{V_W}{V_{dry}} \left(\frac{d}{d_0} \right)^3 \tag{6.19}$$

with d_0 and d respectively being the diameter of the gels in water and in the mixed solvent, we calculated Θ by using V_w/V_{dry} of 20.4.

6.3.3 Permeation Measurements

Mixtures of water (W) and *N*,*N*-dimethylformamide (DMF) with five different compositions, $\varphi_{DMF,\ in}$ = 0, 0.25, 0.50, 0.75 and 1.00, were used as solvents for the permeation measurements. Both solvents are good for PNIPA and have a larger difference in the refractive index. Prior to the measurements the gel membranes were equilibrium-swelled in mixed solvents. Figure 6-2 shows schematic representation of an apparatus used for the permeation measurements. The membranes were sandwiched by two silicone rubber/Teflon mesh composite sheets. A spacer made of the same silicone rubber was also used for the sample setup. The laminar disks were again put into two aluminum plates

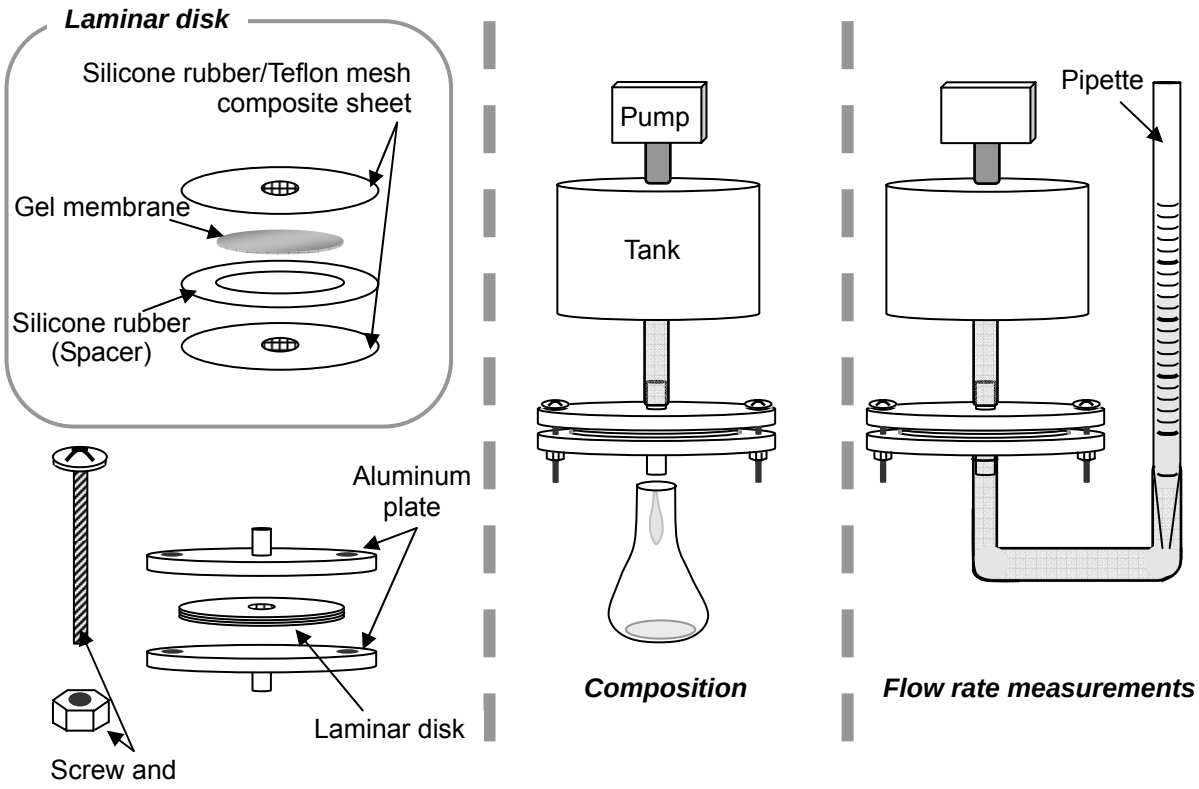

Figure 6-2 The schematic representation of the apparatus used for the flow experiments.

with inlets and the plates were settled by screws. The upper inlet of the apparatus connected to a solvent reservoir tank with a pump. The tank was filled with a large amount of solvent. All measurements were carried out at 20 °C. The values of the applied pressure were monitored by a digital pressure gauge. The pressure was applied by introducing the compressed air to the solvent reservoir. The value p_0 stands for the applied pressure, and is identical to the pressure loss in the gel because the pressure loss in the connection tube was negligibly small (a simple calculation gives the pressure loss of the order of 10^{-5} Pa for the typical setup).

Two types of setup were employed for the bottom part of the aluminum plate. For the solvent composition determination, no tube was connected to the inlet. The solvent composition for the flowed-out solvent was determined by the refractive index of the solvent. The refractive index (n) for the mixed solvents differing in composition was measured in advance by an Abbe refractmeter (NAR-1T, Atago, Japan). The result, a curve relating n to the DMF fraction (φ_{DMF}), is shown in Figure 6-3. This calibration curve was employed to determine φ_{DMF} of the permeated solvents. The effect of the solvent evaporation was ignored because the time required for the measurements was not so long. For the flow rate measurements, the inlet on the bottom side plate was connected to a pipette with reading. The integrated flow rate of the permeated solvent was obtained by the change in readings for the solvent.

6.4 Results and Discussion

Figure 6-4 shows Θ for the PNIPA gels in the mixed solvents as a function of the DMF fraction for the surrounding solvent (φ'_{DMF}). The gel in

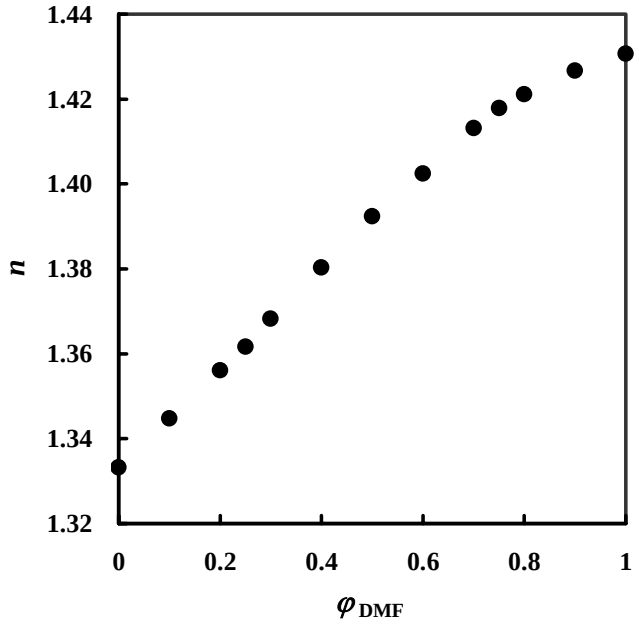

Figure 6-3 Refractive index (n) as a function of the volume fraction of DMF (φ'_{DMF}) in mixed solvents of water and DMF.

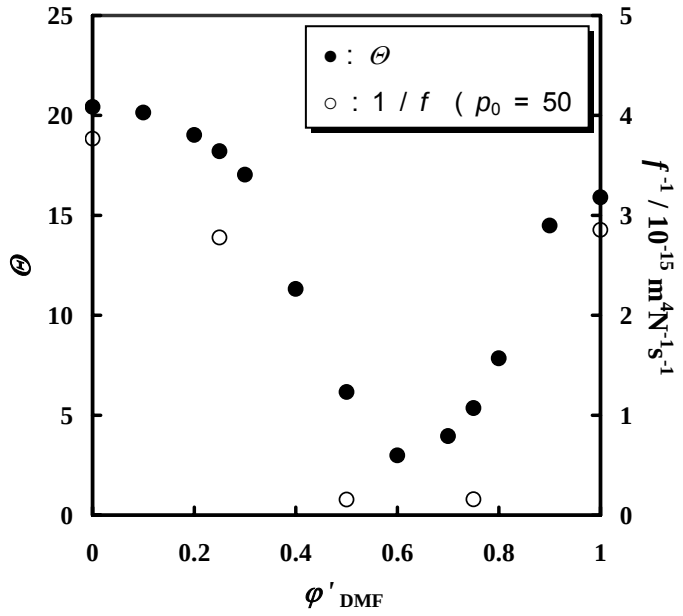

Figure 6-4 Composition dependence of the degree of swelling (Θ) of PNIPA gels in mixed solvents of water and DMF. The figure contains the data of the inverse of the friction coefficient (f).

water ($\varphi'_{DMF} = 0$) is highly swollen ($\Theta \approx 20$) and Θ decreases with increasing φ'_{DMF} in the region of $\varphi'_{DMF} < 0.6$. The minimum ($\Theta \approx 3$) occurs at $\varphi'_{DMF} \approx 0.6$ and then Θ increases again with increasing φ'_{DMF}. Comparing Θ in water and DMF, Θ for water is a little larger than that for DMF, but the difference in Θ is not so large; namely, DMF as well as water appears to be a good solvent for PNIPA. As stated in Section 6.2.1, the model presented here does not ignore the enthalpic interaction between two kinds of solvents. However, the unique behavior on the Θ vs φ'_{DMF} curve, a cononsolvency phenomenon,[19] cannot be explained by this model. To describe the cononsolvency phenomenon the composition dependence must be introduced to the interaction parameters.

Figure 6-5 shows the compositions of the downstream solvents ($\varphi_{DMF, out}$), the solvents flowed out through the PNIPA gel membranes, plotted against the compositions of the upstream solvents ($\varphi_{DMF, in}$) at p_0 = 50 kPa. In the figure a line with a slope of 1 is drawn for reference. The data points fall on the line, indicating that the compositions of the downstream and upstream solvents are almost the same. As stated previously in Figure 6-4, Θ of the gel membranes became rather small in the middle $\varphi_{DMF, in}$ region. Due to the small values of Θ the performance for the solvent separation was expected to increase in this region, but the performance remains almost constant, independently of $\varphi_{DMF, in}$. From the figure it is expected that the composition inside the gel membrane is identical to the composition of downstream (also upstream) solvent. In Figure 6-6 the separation coefficient (α) calculated by Equation (6.1) is plotted against $\varphi_{DMF, in}$. Actually, α lies around 1. From these results, thus, in the flow rate measurements we need not take into account the back-flow from the downstream solvent to the upstream solvent driven by osmotic pressure because

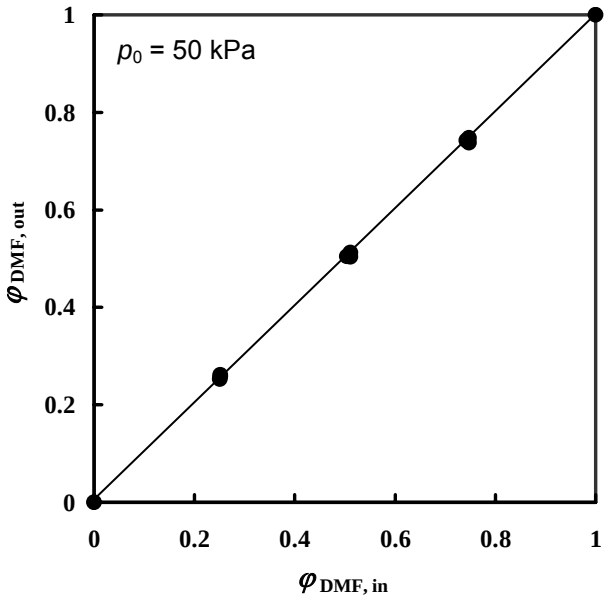

Figure 6-5 Composition of the downstream solvent as a function of composition of the upstream solvent. The measurements were examined thrice at each composition of the mixed solvent, and all the results are shown although the plots are overlapped at the same composition. A line with slope of 1 is drawn for reference.

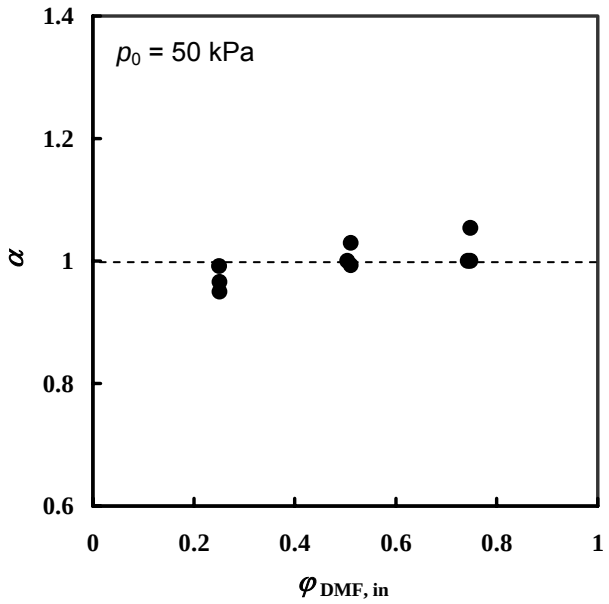

Figure 6-6 Composition dependence of the separation coefficient (α). Three points are plotted at each composition as shown in Figure 6-4.

of the same compositions in the upstream and downstream solvents.

Figure 6-7 shows the integrated solvent flow rate over t (F) through the gel membranes for the upstream solvents at various DMF compositions plotted against time t. At t = 0 a pressure is applied to the solvent reservoir tank. Although the data points are a little scattered (especially, curves in Figure 6-7a), F monotonically increases with t. The slope of the curves decreases with t and then reaches a steady value at long times. The constant slope is attained at ~500 s for the gels swollen by water and at ~5,000 s for the collapsed gel with φ_{DMF} = 0.5. The decrease of the slope, equivalent to the decrease in the flow rate, results from the re-swelling of the gel membrane by flow.[13] Actually, the equilibration time τ calculated by $\tau = d^2/D$ for re-swelling is not so far from the experimental one for the gels in the collapsed as well as swollen state (τ = ~10^3 s for both states), if we calculate the diffusion constant by using the Young's modulus of 10^5 Pa (for the gels in the collapsed state) and 10^4 Pa (for the gels in the swollen state).[2, 20] In the cases of pure water ($\varphi_{DMF, in}$ = 0: $\varphi_{DMF, in}$; the DMF fraction in the upstream solvent) and pure DMF ($\varphi_{DMF, in}$ = 1), the effects of pressure on F was investigated (Figures 6-7a and 6-7c). An increase of the applied pressure enhances the flow rate for both solvents. This agrees with the model prediction in Equation (6.16): Q is proportional to p_0. In order to compare the steady flow rate Q at various solvent compositions, it is convenient to introduce the total frictional coefficient f in the steady state.

$$f \equiv \frac{p_0}{Qd} \tag{6.20}$$

where d and P_0 represent the thickness and the applied pressure, respectively. We used d in the swollen state for each composition. We obtained the degree of

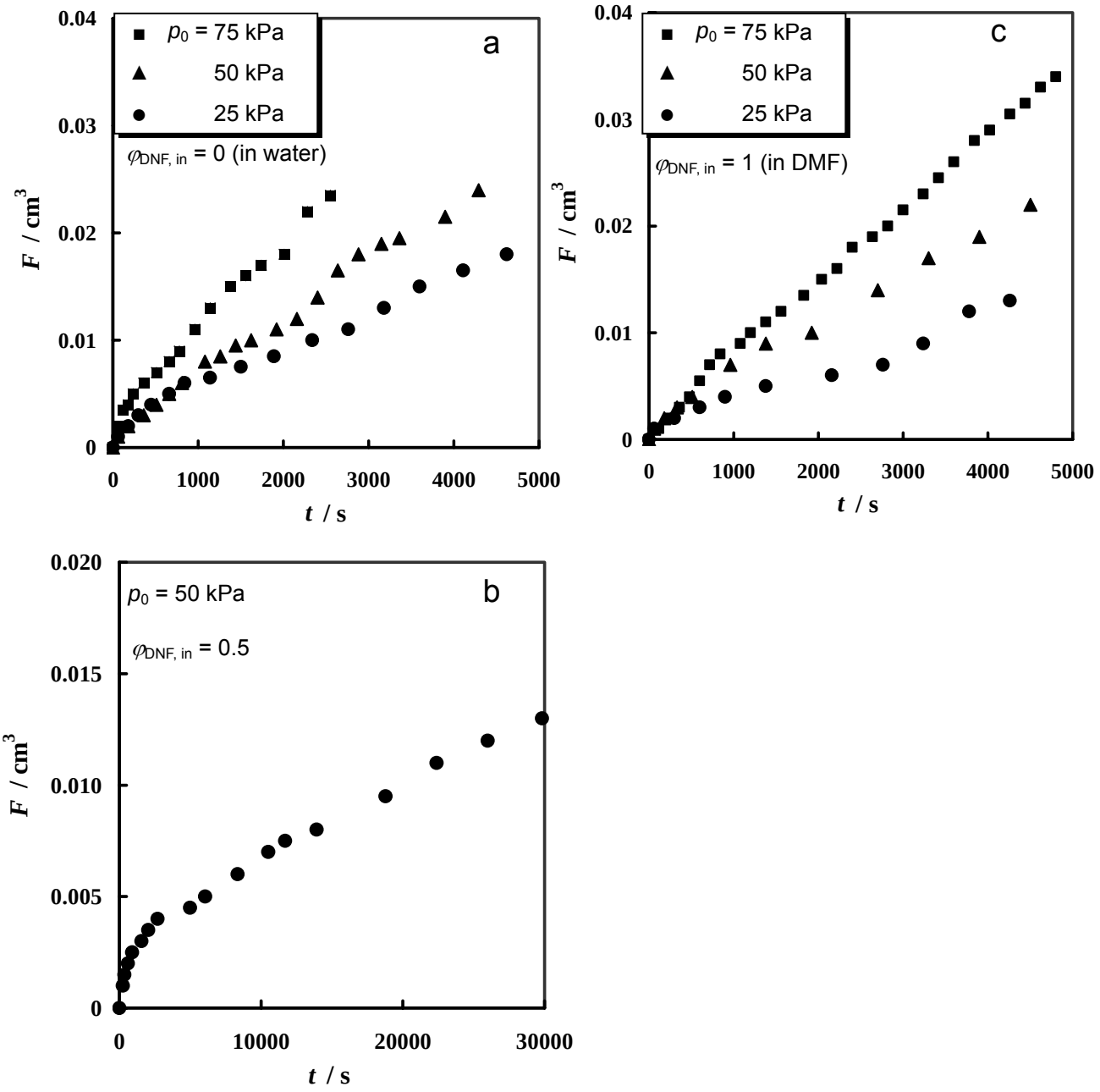

Figure 6-7 Integrated flow rate over time as a function of time in water (A), in mixed solvents of water and DMF at φ_{DMF} = 0.5 (B) and in DMF (C).

swelling at each composition, and the upstream and downstream composition was eventually the same. The thickness of the sample was calculated by the value of d for pure water and the degree of swelling at each composition. Figure 4 also contains the values of $1/f$ at p_0 = 50 kPa. The shape of the $1/f$ curve is quite similar to that of the Θ curve. Comparing the values of $1/f$ at $\varphi_{DMF,\,in}$ = 0 and $\varphi_{DMF,\,in}$ =1, $1/f$ at $\varphi_{DMF,\,in}$ = 0 is slightly larger than that at $\varphi_{DMF,\,in}$ = 1, meaning that f at $\varphi_{DMF,\,in}$ = 0 (f_W) is smaller than that at $\varphi_{DMF,\,in}$ = 1 (f_{DMF}). The friction coefficient f is considered to be proportional to the solvent viscosity η. The viscosities of DMF and water at 20 ^oC are reported to be 0.9243 mPas and 1.0019 mPas, respectively.[21] This leads to the opposed relation for the experiments, probably resulting from the difference in Θ for the two solvents. According to the two-fluid model shown in Section 6.2.2., where the polymer concentration is implicitly assumed to be constant, f is given from Equation (6.16) by using the DMF composition inside the gel (φ_{DMF}) as $1/f = (\varphi_{DMF} / f_{DMF}) + (1 - \varphi_{DMF}) / f_W$. This suggests a monotonic function of φ_{DMF} for $1/f$ when the comparison is made under a constant polymer concentration. The shape of the $1/f$ curve in Figure 6-3, however, is not monotonic. This permeation behavior cannot be explained by the two-fluid model. Of course, the controlled variable in the figure is not φ_{DMF} but $\varphi_{DMF,in}$, but they are expected to be almost the same, as described before. The large friction coefficients in the middle range of $\varphi_{DMF,in}$ originate mainly from the shrinkage of the gel membranes; namely, the decrease in the mesh size of the polymer networks.

The solvent composition inside the PNIPA gels cannot be obtained directly by experiments. However, we can estimate the solvent composition inside gels if Equation (6.16) is valid. In this case, the following equations can

be used for the estimation.

$$\frac{\varphi_{\mathrm{DMF}}}{\varphi_{\mathrm{W}}} = \frac{\varphi_{\mathrm{DMF,out}}}{\varphi_{\mathrm{W,out}}} \cdot \frac{f_{\mathrm{DMF}}}{f_{\mathrm{W}}} \tag{6.21a}$$

$$\varphi_{\mathrm{W}} + \varphi_{\mathrm{DMF}} = \varphi_{\mathrm{W,out}} + \varphi_{\mathrm{DMF,out}} = 1 \tag{6.21b}$$

The calculated values of the DMF fraction inside the gels φ_{DMF} are illustrated in Figure 6-8. A solid line in the figure has a slope of 1. The data points again fall around the line, indicating that the volume fraction of DMF inside the gels is almost the same as that of the upstream solvent, as in the case of Fig. 6-5. Based on the results in Fig. 6-8, it is also suggested that the surrounding and inside solvents have the same composition for the PNIPA gels for the water/DMF binary solvent system when the gels are immersed into the mixed solvents for swelling.

6.5 Conclusions

We investigated the flow properties of mixed solvents of water and DMF through PNIPA gel membranes. The swelling behavior of the gels in the mixed solvents was also examined. A simple model to explain the swelling and solvent flow properties for a polymer gel/mixed solvent system was presented. The composition dependence of the degree of swelling (Θ) of the PNIPA gels in the mixed solvents was not linear and showed a minimum at about φ'_{DMF} of 0.6. Pressure gradient acting between two solvent-gel interfaces allowed the permeation of the mixed solvents through the gel membranes. Little change in solvent composition by the permeation through the membranes occurred even at

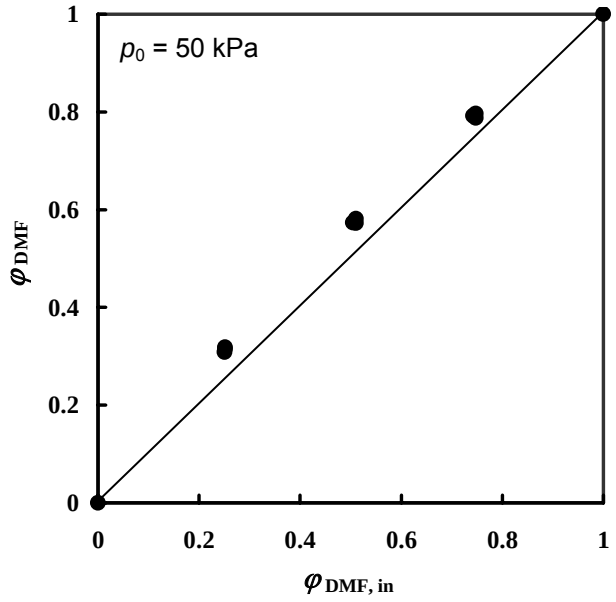

Figure 6-8 Composition of the solvent inside gels as a function of composition of the upstream solvent. Since this calculation results were obtained from the results of Figure 6-4, three points are plotted at each composition of the mixed solvent. A line in the figure is of a slope of 1.

compositions where the Θ vs composition curve showed a minimum. The integrated flow rate over t (F) monotonously increased with increasing t. The slope of F vs t curves decreased with time and then becomes constant at long times. The inverse of the frictional coefficients for the steady flow plotted against solvent composition is quite similar in shape to the Θ curve. This reveals that the degree of the swelling greatly affects the flow rate of the solvents in the gels. The calculation on the basis of the model also suggests that the composition inside the gel is equal to the composition of the surrounding solvent.

References

1. S. Hirotsu, *Macromolecules*, **37**, 3415 (2004)
2. T. Takigawa, T. Yamawaki, K. Takahashi, and T. Masuda, *Polymer Gels and Networks*, **5**, 585 (1997)
3. T. Takigawa, T. Ikeda, Y. Takakura, and T. Masuda, *J. Chem. Phys.*, **117** 7306 (2002)
4. T. Tanaka, D. Fillmore, S. Sun, I. Nishio, G. Swislow, and A. Shah, *Phys. Rev. Lett.*, **45**,1636 (1980)
5. Y. Hirokawa, and T. Tanaka, *J. Chem. Phys.*, **81**, 6379 (1984)
6. S. Hirotsu, *J. Phys. Soc. Jpn.*, **56**, 233 (1987)
7. S. Hirotsu, Y. Hirokawa, and T. Tanaka, *J. Chem. Phys.*, **87**, 1392 (1987)
8. S. Hirotsu, *J. Chem. Phys.*, **88**, 427 (1988)
9. K. Mukae, M. Sakurai, S. Sawamura, K. Makino, S. W. Kim, I. Ueda, and K. Shirahama, *J. Phys. Chem.*, **97**, 737 (1993)
10. H. Shirota, K. Ohkawa, N. Kuwabara, N. Endo, and K. Horie, *Macromol. Chem. Phys.*, **201**, 2210 (2000)
11. K. Yoshimura, and K. Sekimoto, *J. Chem. Phys.*, **101**, 4407 (1994)
12. T. Ishidao, Y. Hashimoto, Y. Iwai, and Y. Arai, *Colloid Polym. Sci.*, **272**, 1313 (1994)
13. T. Takigawa, K. Uchida, K. Takahashi, and T. Masuda, *J. Chem. Phys.*, **111**, 2295 (1999)
14. M. Tokita, and T. Tanaka, *J. Chem. Phys.*, **95**, 4613 (1991)
15. M. Tokita, and T. Tanaka, *Science*, **253**, 1121 (1991)
16. Y. Doi, and M. Tokita, *Langmuir*, **21**, 9420 (2005)

17. A. Suzuki, and M. Yoshikawa, *J. Chem. Phys.*, **125**, 174901 (2006)

18. P. J. Flory, “Principles of Polymer Chemistry”, Cornell University Press, Ithaca, NY, 1953

19. H. G. Schild, M. Muthukumar, and D. A. Tirrell, *Macromolecules*, **24**, 948 (1991)

20. T. Takigawa, K. Urayama, Y. Morino, and T. Masuda, *Polymer Journal*, **25**, 929 (1993)

21. J. A. Riddick and W. B. Bunger, “Techniques of Chemistry: Vol. 2, Organic Solvents 3rd edition”, John Wiley & Sons, Inc., NY, 1970

Summary

In Chapter 1, the historical background and the motivation of this study were described. The thermodynamics and kinetics of swelling and shrinking of polymer gels were reviewed. The effects of the external forces on the swelling and shrinking behavior were also stated. The problems that to be solved were pointed out.

In Chapter 2, the effects of static and dynamic loading on the swelling properties of poly(*N*-isopropylacrylamide) (PNIPA) hydrogels in the swollen state were investigated by using a laboratory-made magnetic force-driven rheometer. In the static measurements, the gel under a constant stress underwent the stress-induced swelling, and the Poisson ratio decreased with time. In the dynamic measurements using sinusoidally oscillating forces, the swelling behavior of the gels in water depended on the measuring frequency (ω) while that in liquid paraffin (non-solvent for PNIPA) was independent of ω like elastic rubbers. The dynamic Poisson ratio significantly depended on ω due to the stress-induced swelling with a characteristic time. The dynamic Poisson ratio at $\omega \to \infty$ (short time limit) or $\omega \to 0$ (long time limit) agreed well with the corresponding Poisson's ratio obtained by the static tests. The phase lags of strain seeing from the stress showed a peak at a certain angular frequency. The inverse of the frequency was identical with the characteristic time of stress-induced swelling observed in the static tests.

In Chapter 3, the static and dynamic swelling behavior of the

PNIPA hydrogels in the collapsed state was investigated by using the same apparatus as Chapter 2. In the static tests, the applied stress caused the creep behavior of the gel in water, namely the length and the diameter of the gels gradually increased and decreased with time, respectively. When the stress was released, the gel recovered the original state before deformation. The creep and creep recovery behavior originated from the destruction and generation of the hydrogen bonds in the deformed gel. Under constant strains, a small but definite stress-induced swelling was observed. The deformation of the PNIPA gel in the collapsed state was mainly governed by the creep behavior while that in the swollen state was dominated by the stress-induced swelling after instantaneous deformation. In the dynamic measurements, the amplitude of the displacement in length decreased and the phase lag increased as angular frequency increases. The retardation spectrum could be expressed by the multi-type retardation function with almost identical intensities. The static data was reproduced by the conversion of the dynamic data.

In Chapter 4, the shrinking behavior of polyacrylamide (PAAm) gels induced by ultracentrifugal field were investigated. A theory was proposed to describe the diffusion process of networks in the presence of centrifugal fields. The theory predicts that the initial shrinking rate is governed by the ratio of the frictional force and the centrifugal force and that the stationary shrinkage is determined by the balance between the elastic force and the centrifugal force. The whole shrinking process in the experiments was described by a single exponential relaxation whose

characteristic time is proportional to the ratio of the square of the stationary displacement and the diffusion constant of networks, in agreement with the theoretical expectation. In the initial region, the gel was shrunken at a constant rate, while the shrinking reached the stationary state in the long time limit. On the basis of the theory, the friction constant as well as the longitudinal elastic modulus of the network were successfully estimated.

In Chapter 5, the shrinking behavior of the poly(vinyl alcohol) (PVA) physical gels under ultracentrifugal forces was investigated by the same method in Chapter 4. The shrinking process of PVA physical gels were qualitatively similar to that of PAAm chemical gels: The shrinking velocity was constant at the initial stage and the shrinkage reaches the stationary state in the long time limit. The change of the polymer network density in course of the shrinking qualitatively agreed with the theoretical prediction. The shrinking velocity v was proportional to the square of the rotational speed ω ($v \propto \omega^2$), in accordance with the theoretical expextation. The frictional coefficient f of the PVA gels was estimated on the basis of the theory. The results in Chapters 4 and 5 suggested that a ultracentrifuge is useful for the measurement of the frictional coefficient of polymer gels.

In Chapter 6, the flow properties of mixed solvents of water and *N*,*N*-dimethylformamide (DMF) through PNIPA gel membranes were investigated. The swelling ratio of the gels in the mixed solvents was also examined. A simple model to describe the swelling and solvent flow properties for a polymer gel/mixed solvent system was presented. The degree of swelling (Θ) was dependent on the solvent composition and

showed a minimum at about DMF volume fraction of 0.6. The pressure gradient acting on the gel membrane caused the permeation of the mixed solvents through the gel. The composition of the permeation solvent that flowed out through the gel membrane was almost the same as that of the upstream solvent. The integrated flow rate over t (F) monotonously increased with time. The slope of F vs t curves decreased with time and then became constant at long times. The degree of the swelling greatly affected the flow rate of the solvents. The composition inside the gel was calculated from the proposed model, and the composition was estimated to be almost identical with that of the surrounding solvent.

List of Publication

Papers Rated to the Present Dissertaion

1. “Dynamic Swelling Properties of a Poly(*N*-isopropylacrylamide) Gel Measured by a Magnetic Force-driven Rheometer”
   Takigawa T, Nosaka S, Takakura Y, Urayama K, *Polymer Journal*, **35**, 819 (2003) (Chapter 2)
2. “Static and Dynamic Swelling Properties of Poly(*N*-isopropylacrylamide) Gels in the Swollen State”
   Nosaka S, Urayama K, Takigawa T, *Polymer Journal*, **37**, 694 (2005) (Chapter 2)
3. “Creep Behavior of Poly(*N*-isopropylacrylamide) Gels in the Collapsed State”
   Nosaka S, Urayama K, Takigawa T, *Polymer Journal*, **38**, 970 (2006) (Chapter 3)
4. “Kinetics of Shrinking of Polymer Gels Induced by Ultracentrifugal Fields”
   Urayama K, Okada S, Nosaka S, Watanabe H, Takigawa T, *J. Chem. Phys.*, **122**, 024906 (2005) (Chapter 4)
5. “Compression of Poly(vinyl alcohol) Gels by Ultracentrifugal Forces”
   Nosaka S, Okada S, Takayama Y, Urayama K, Watanabe H, Takigawa T, *Polymer*, **46**, 12607 (2005) (Chapter 5)
6. “Steady Flow Properties of a Mixed Solvent through a Poly(*N*-isopropylacrylamide) Gel”

Nosaka S, Ishida T, Urayama K, Takigawa T, *J. Mem. Sci.*, **305**, 325 (2007) (Chapter 6)

Acknowledgment

This dissertation has been written on the basis of the research carried out at Department of Material Chemistry, Graduate School of Engineering, Kyoto University, from 2002 to 2007 under the guidance of Professor Toshikazu Takigawa. The author wishes to express his sincere gratitude to Professor Toshikazu Takigawa for his continuous guidance, encouragement and valuable comments.

The author is sincerely grateful to Dr. Kenji Urayama and Dr. Jun-ichi Horinaka for their instructive discussion, helpful advice and collaborations throughout this study.

The author acknowledges Mr. Shinichi Okada and Professor Hiroshi Watanabe, Institute for Chemical Research, Kyoto University, for their collaboration in the experiments.

The author would also thank Professor Shunsaku Kimura, Department of Material Chemistry, Graduate School of Engineering, Kyoto University, and Professor Fumihiko Tanaka, Department of Polymer Chemistry, Graduate School of Engineering, Kyoto University, for their careful reading and detailed criticism to this dissertation.

Thanks are also due to all members, past and current, of Takigawa laboratory including Messrs. Yoshihito Takakura, Yoshiyuki Takayama and Takuya Ishida for their kind help during this study.

Shoji Nosaka

Kyoto, Japan

December, 2007